Realization of Thermally Stimulated Delay Phosphorescence in Arylgold(III) Complexes and Efficient Gold(III) Based Blue-Emitting OLEDs

Man-Chung Tang,[‡] Ming-Yi Leung,[‡] Shiu-Lun Lai, Maggie Ng, Mei-Yee Chan, Vivian Wing-Wah Yam**

[*] Dr. M.-C. Tang, Ms. M.-Y. Leung, Dr. S.-L. Lai, Dr. M. Ng, Dr. M.-Y. Chan,* Prof. V. W.-W. Yam*
Department of Chemistry, The University of Hong Kong, Pokfulam Road, Hong Kong.
Fax: +(852) 2857-1586; Tel: +(852) 2859-2153
E-mail: wwyam@hku.hk; chanmym@hku.hk

[‡] Both authors contributed equally to this work.

Table of Contents

Experimental details

Physical measurements and instrumentation

The UV-vis absorption spectra were recorded on a Cary 60 UV-vis (Agilent Technology) spectrophotometer equipped with a Xenon flash lamp. ^{1}H and $^{13}C\{^{1}H\}$ NMR spectra were recorded on a Bruker Avance 500 (500 MHz for ^{1}H and 100 MHz for $^{13}C\{^{1}H\}$ nuclei) or Bruker Avance 600 (600 MHz for ^{1}H or 150 MHz for $^{13}C\{^{1}H\}$ nuclei) Fourier-transform NMR spectrometer with chemical shifts reported relative to tetramethylsilane (δ = 0 ppm) in chloroform. $^{19}F\{^{1}H\}$ NMR spectra were recorded on a Bruker Avance 400 (376 MHz for ^{19}F nucleus) Fourier-transform NMR spectrometer with chemical shifts reported relative to trifluoroacetic acid ($\delta = -76.55$ ppm) in chloroform. UV-Vis absorption spectra were recorded on a Varian Cary 50 spectrophotometer equipped with a Xenon flash lamp. Steady-state emission spectra were recorded using an Edinburgh Instruments FS5 Spectrofluorometer. Liquid nitrogen was placed into the quartz-walled optical Dewar flask for low temperature (77 K) photophysical measurements. Solid-state photophysical measurements were performed with solid sample loaded into a quartz tube inside a quartz-walled optical Dewar flask. Low temperature (77 K) photophysical measurements were done by placing liquid nitrogen into the optical Dewar flask. Excited-state lifetimes of solution and glass samples were measured with a conventional laser system. The excitation source used was the 355 nm output (third harmonic, 8 ns) of a Spectra-Physics Quanta-Ray Q-switched GCR-150 pulsed Nd:YAG laser (10 Hz). Luminescence decay signals were recorded by a Hamamatsu R928 photomultiplier tube, recorded on a Tektronix model TDS-620A (500 MHz, 2 GSs^{-1}) digital oscilloscope, and analyzed with a program for exponential fits. Relative photoluminescence quantum yields in solution were measured by the optical dilute method reported by Demas and Crosby.[1] An aqueous solution of quinine sulfate in 1.0 N H_2SO_4 has been used as the reference ($\Phi_{lum} = 0.546$, excitation wavelength at 365 nm),[1] whereas absolute photoluminescence quantum yields in thin films and solids were measured on a Hamamatsu C9920-03 absolute PLQY measurement system. Excited-state lifetimes of thin films and solids were measured on a Quantaurus-Tau C11367-34 fluorescence lifetime spectrometer. Variable-temperature emission spectra were obtained using the Edinburgh Instruments FS5 Spectrofluorometer with an Oxford Instrument OptistatDN2 cryostat for temperatures in the range of 77 K to 300 K. The solid sample was placed in a quartz cell inside the cryostat and maintained at the desired temperature until equilibrium was reached before recording the spectrum. Variable-temperature excited state lifetimes were measured on a Quantaurus-Tau C11367-34 fluorescence lifetime spectrometer.

The solid sample was placed in a quartz cell inside an Oxford Instrument OptistatDN2 cryostat for temperatures in the range of 77 K to 300 K. Cyclic voltammetry was performed with a CH Instruments Model CHI620E (CH Instruments, Inc.) electrochemical analyzer. All solutions for electrochemical measurements were purged with pre-purified argon gas prior to measurement. Thermal analyses were performed on a TGA Q50 (TA Instruments), in which T_d is defined as the temperature at which the sample shows a 5 % weight loss.

X-Ray crystallography

The crystal samples for complexes **1**–**3** were obtained as needles. The crystal data were collected on a Bruker D8 VENTURE FIXED-CHI PHOTON 100 CMOS X-Ray Diffractometer using molybdenum Mo-Kα (λ = 0.71073 Å) X-ray source. The structure was solved by direct methods employing SHELXT2014 program and refined by full-matrix least-squares by using the program SHELXL2014.[2] The crystal data for complexes **1**–**3** are summarized as shown in Table S11. The X-ray crystallographic data for complexes **1**–**3** have been deposited at the Cambridge Crystallographic Data Centre (CCDC), under the deposition number CCDC 1842615, CCDC 1842617, CCDC 1842616. These data can be obtained free of charge from The Cambridge Crystallographic Data Center via www.ccdc.cam.ac.uk/data_request/cif.

DFT and TDDFT computational calculations

All calculations were carried out with the Gaussian 09 program suite.[3] The ground (S_0) state geometries of complexes **1**−**4** were fully optimized in dichloromethane by DFT method with the hybrid Perdew, Burke, and Ernzerhof (PBE0) functional,[4–6] in conjunction with the conductor-like polarizable continuum model (CPCM).[6,7] On the basis of the optimized S_0 geometries, TDDFT method[8–10] at the same level associated with CPCM (CH_2Cl_2) was employed to compute the singlet−singlet transitions. To gain more insight into the emissive states, unrestricted UPBE0 method was employed to compute the singlet−triplet transitions. Vibrational frequency calculations were performed on all stationary points to verify that each was a minimum (NIMAG = 0) on the potential energy surface. For all the calculations, the Stuttgart effective core potentials (ECPs) and the associated basis set were utilized to describe Au[11] with f-type polarization functions (ζ = 1.050),[12] while the 6-31G(d,p) basis set[13–15] was applied for all other atoms. All DFT and TDDFT calculations were performed with a pruned (99,590) grid for numerical integration.

Device fabrication and characterization

Solution-processed OLEDs were fabricated on patterned ITO coated glass substrates with a sheet resistance of 30 Ω per square. The substrates were cleaned with Decon 90, rinsed with deionized water, dried in an oven, and finally treated in an ultraviolet-ozone chamber. A 40 nm thick poly(ethylenedioxythiophene):poly(styrene sulfonic acid) (PEDOT:PSS) layer was spin-coated onto the ITO coated glass substrates as hole-transporting layer. After that, the emissive layer was formed by mixing the gold(III) complex with MCP to prepare a 10 mg cm^{-3} solution in chloroform and spin-coated onto the PEDOT:PSS layer to give uniform thin films of 30 nm thickness. Onto this, a 5-nm thick tris(2,4,6-trimethyl-3-(pyridine-3-yl)phenyl)borane (3TPyMB) and a 40-nm thick 1,3,5-tri[(3-pyridyl)-phen-3-yl]benzene (TmPyPB) were evaporated as a hole-blocking layer and an electron-transporting layer, respectively; while LiF/Al was used as the metal cathode. For the vacuum-deposited OLEDs, sequential thermal evaporation of *N*,*N*'-bis(naphthalene-1-yl)-*N*,*N*'-bis(phenyl)-2,2'-dimethylbenzidine (α-NPD; 40 nm), emissive layer (25 nm), diphenyl-4-triphenylsilylphenyl-phosphine oxide (TSPO1; 5 nm) 1,3,5-tris(6-(3-(pyridin-3-yl)phenyl)pyridine-2-yl)benzene (Tm3PyP26PyB; 35 nm), LiF (1 nm) and Al (100 nm) were made onto the ITO substrate, in which α-NPD, TSPO1, and Tm3PyP26PyB were used as hole-transporting, exciton-blocking and electron-transporting layers, respectively. The emissive layer was prepared by co-evaporating the respective gold(III) complex and 2,6-di(9*H*-carbazol-9-yl)pyridine (PYD-2Cz) as host simultaneously. Particularly, the deposition rate of the PYD-2Cz was kept at 0.2 nm s^{-1} while that of the dopant was adjusted from 0.004–0.028 nm s^{-1}, depending on the desired concentration. All organic materials and metals were thermally evaporated by a Trovato vacuum deposition system in vacuum under a base pressure of 10^{-6} Torr. High-purity 3TPyMB, TmPyPB, MCP, α-NPD, TSPO1, Tm3PyP26PyB and PYD-2Cz (>99.5 % HPLC) were purchased from Luminescence Technology Corporation and were used as received. All films were sequentially deposited at a rate of 0.1−0.2 nm s^{-1} without vacuum break. A shadow mask was used to define the cathode and to make four 0.1 cm^2 devices on each substrate. Current density−voltage−luminance characteristics and EL spectra were measured simultaneously with a programmable Keithley model 2400 power source and a Photoresearch PR-655 spectrometer. All the devices were measured under ambient conditions without encapsulation. For operational stability testing, vacuum-deposited device with the configuration of ITO/dipyrazino[2,3-f:2',3'-*h*]quinoxaline-2,3,6,7,10,11-hexacarbonitrile (HAT-CN; 10 nm)/*N*,*N*'-bis(naphthalen-1-yl)-*N*,*N*'-bis(phenyl)-2,2'-dimethylbenzidine (α-NPD; 40 nm)/9,9',9''-triphenyl-9*H*,9'*H*,9''*H*-3,3':6',3''-tercarbazole (TrisPCz; 10 nm)/8 % **1**:PYD-2Cz (25 nm)/2,4,6-tris[3-

(diphenylphosphinyl)phenyl]-1,3,5-triazine (T2T; 10 nm)/2,7-di(2,2'-bipyridin-5-yl)triphenylene (BPyTP2; 40 nm)/LiF (1 nm)/Al (150 nm) had been fabricated and encapsulated in a glovebox under nitrogen. Particularly, the emissive layer was prepared by co-evaporating complex **1** and PYD-2Cz with deposition rates of 0.016 nm s^{-1} and 0.2 nm s^{-1}, respectively. The initial brightness of the encapsulated device was measured by a Keithley 2400 power source and a Photoresearch PR-655 spectrometer; while the operational lifetime of the vacuum-deposited device was measured by a McScience OLED lifetime system by accelerated lifetime testing under a constant driving current density of 10 mA cm^{-2}.

Thermogravimetric analysis

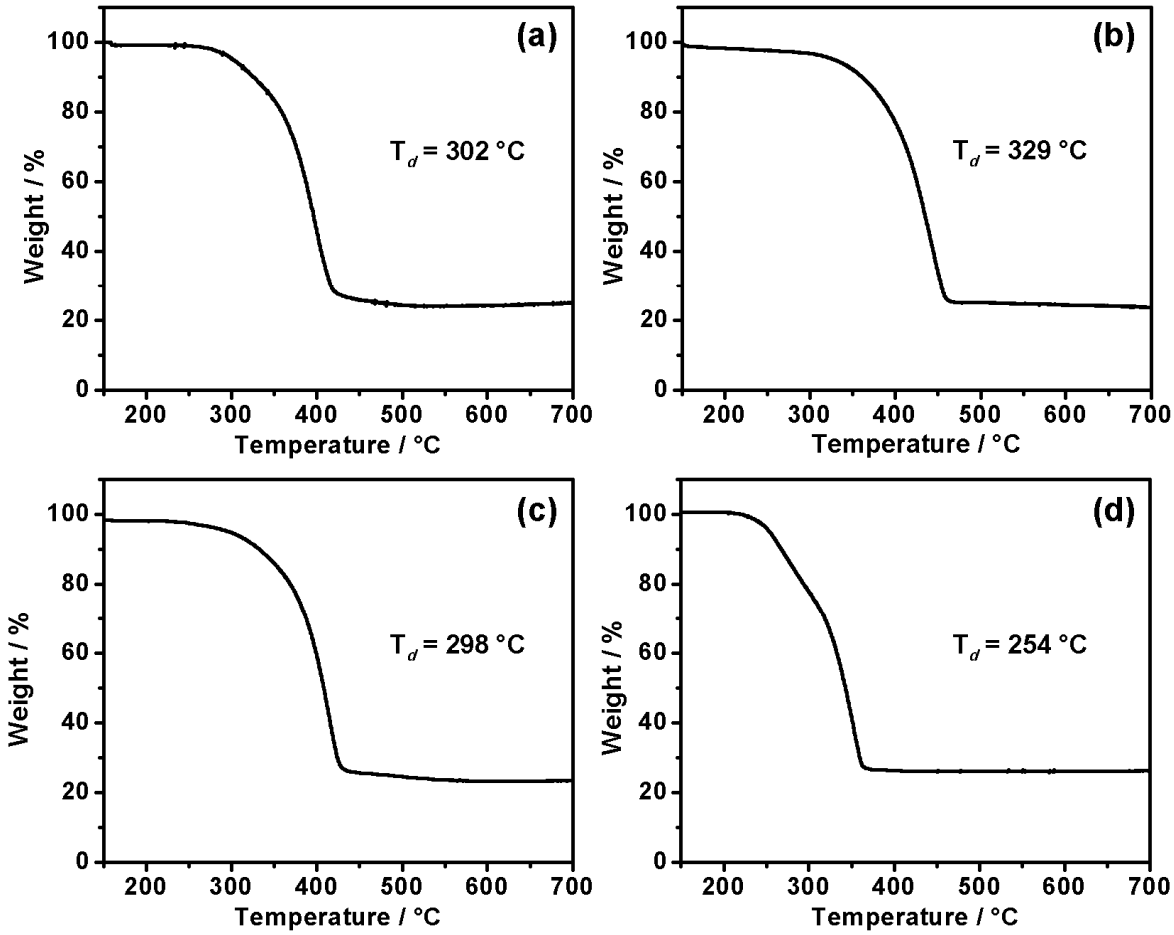

Figure S1. Thermogravimetric analysis (TGA) curves of (a) **1**, (b) **2**, (c) **3** and (d) **4**.

Electrochemical studies

The cyclic voltammetry of **1**−**4** in dichloromethane (0.1 mol dm^{-3} $^{n}Bu_4NPF_6$) has been investigated. Estimations of their HOMO and LUMO energy levels have also been made. The electrochemical data of **1**−**4** are summarized in Table S1, and the cyclic voltammograms of **3** are shown in Figure S2 as an example. An irreversible oxidation wave ranging from +1.80 V to +2.19 V vs standard calomel electrode (SCE) is found for **1**–**4**. The oxidation shows a dependence on the nature of aryl ligands. With a more electron-donating aryl ligand of $–C_6H_4–{}^{t}Bu$ in **2**, a less positive potential for oxidation is observed when compared to that of $–C_6H_3F_2$ and $–C_6H_4–CF_3$ in **1**, **3** and **4** [i.e., **1** (+2.04 V vs SCE), **2** (+1.80 V vs SCE), **3** (+2.00 V vs SCE) and **4** (+2.19 V vs SCE)]. These oxidation waves are assigned as aryl ligand-centered oxidations.[16] In the reductive scan, all the complexes show a quasi-reversible reduction couple at –1.26 V to –1.51 V vs SCE and an irreversible reduction wave at –1.83 V to –2.00 V vs SCE. The first reduction couple is found to show no changes towards the nature of the aryl ligands, [i.e. **1**–**3** (*ca.* –1.30 V vs SCE)], but become significantly more negative with a less electron-donating pincer ligand [i.e. **4** (–1.51 V vs SCE)]. Hence, the reduction waves are assigned as the ligand-centered reduction of the cyclometalated $C^N^{TRZ}^C$ ligand.[17,18] These results are in line with the photophysical studies.

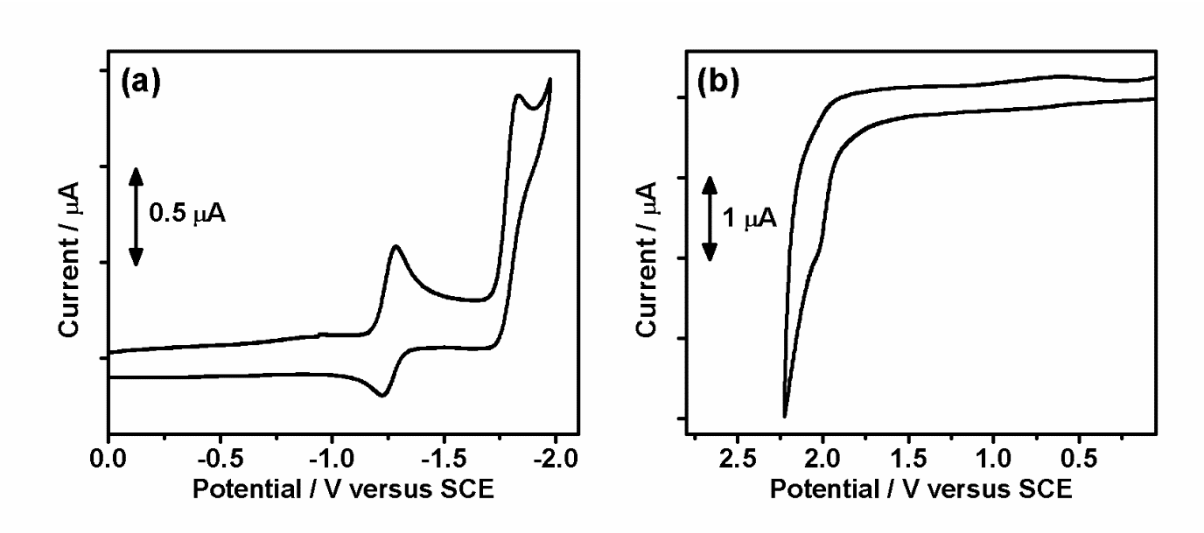

Figure S2. Cyclic voltammograms for (a) reductive and (b) oxidative scans of **3** in degassed CH_2Cl_2 solution (0.1 M $^nBu_4NPF_6$) at 298 K.

Table S1. Electrochemical data for complexes **1**−**4**[a]

Complex	Oxidation [E_{pa} / V vs SCE][b]	Reduction $E_{1/2}$ / V vs SCE[c] (ΔE_p / mV)[d] [E_{pc} / V vs SCE][e]	E_{HOMO} / eV[f]	E_{LUMO} / eV[f]
1	[+2.04]	–1.26 (54), [–1.92]	–6.84	–3.54
2	[+1.80]	–1.32 (80), [–2.00]	–6.57	–3.48
3	[+2.00]	–1.26 (69), [–1.83]	–6.80	–3.54
4	[+2.19]	–1.51 (129)	–6.99	–3.29

[a] In CH_2Cl_2 solution with 0.1 M $^nBu_4NPF_6$ (TBAH) as supporting electrolyte at 298 K; working electrode, glassy carbon; scan rate = 100 mV s^{-1}. [b] E_{pa} refers to the anodic peak potential for the irreversible oxidation waves. [c] $E_{1/2} = (E_{pa} + E_{pc})/2$; E_{pa} and E_{pc} are the peak anodic and peak cathodic potentials, respectively. [d] $\Delta E_p = (E_{pa}–E_{pc})$. [e] E_{pa} refers to the anodic peak potential for the irreversible oxidation waves. [f] E_{HOMO} and E_{LUMO} levels were calculated from the redox potentials of the first oxidation and reduction waves respectively, that is, $E_{HOMO} = –e(4.8\ V + E_{pa})$; $E_{LUMO} = –e(4.8\ V + E_{pc})$.

UV-Vis absorption and emission properties

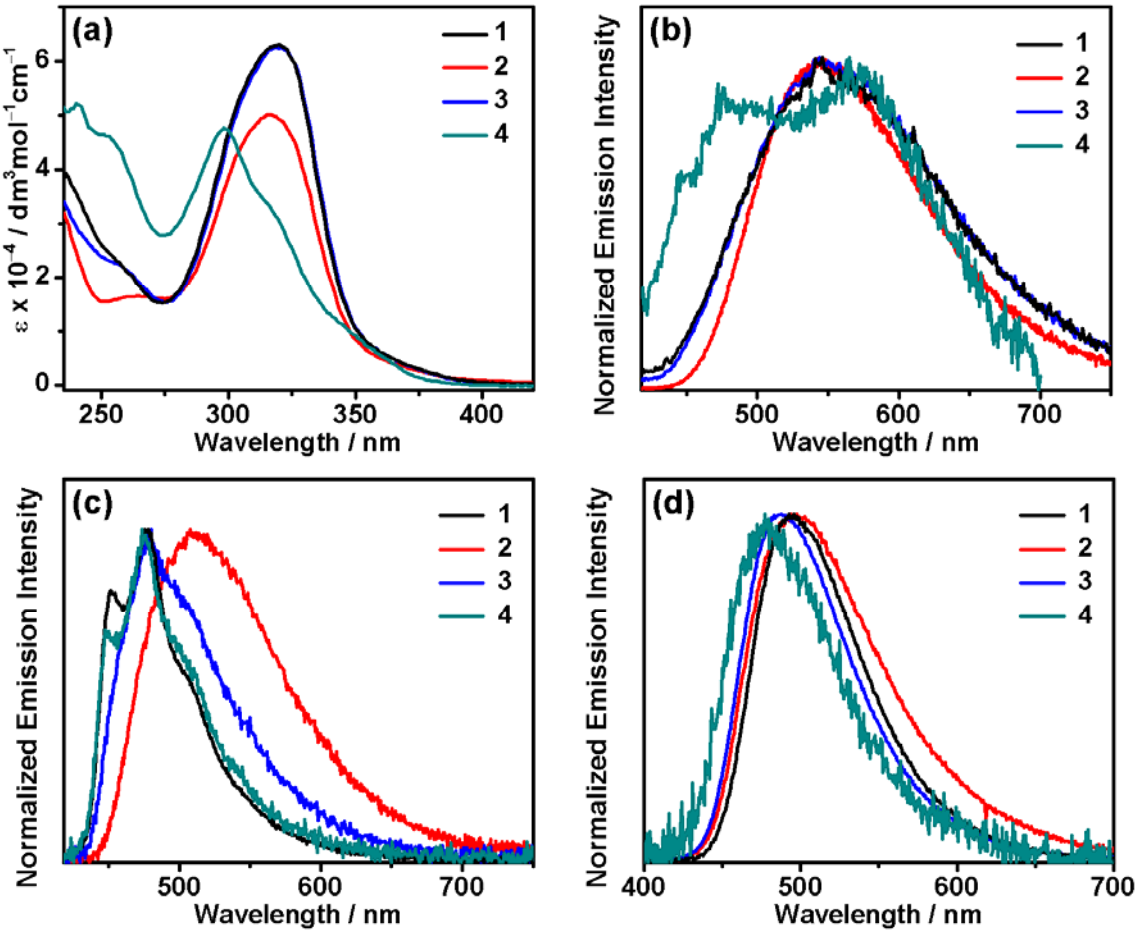

Figure S3. (a) UV-visible absorption spectra and (b) emission spectra of **1**−**4** in degassed dichloromethane at 298 K; (c) solid state emission spectra of **1**−**4** at 298 K; (d) emission spectra of solution-processed films of 20 wt% of **1**–**4** doped into MCP host at 298 K.

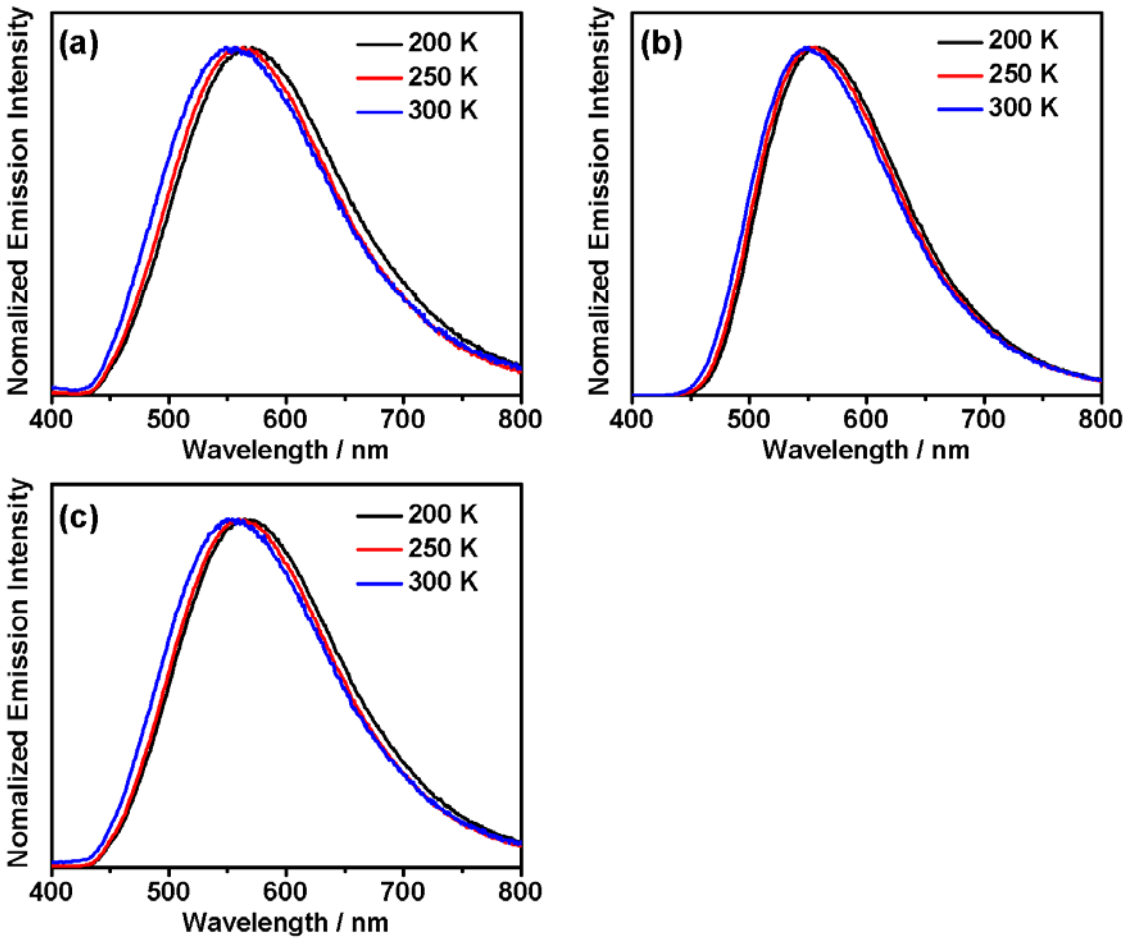

Figure S4. Normalized emission spectra of (a) **1**, (b) **2** and (c) **3** in dichloromethane at different temperatures between 200 K and 300 K upon excitation at 340 nm.

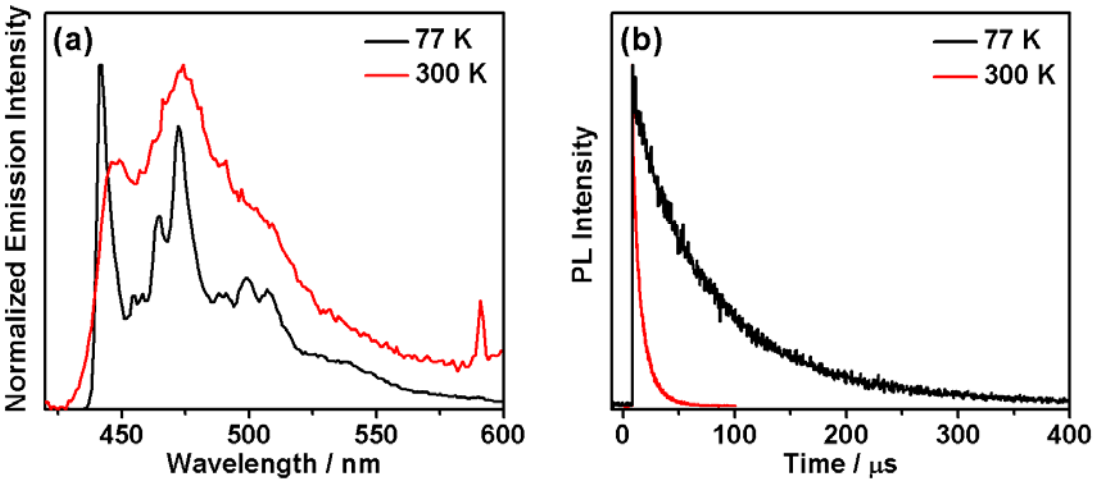

Figure S5. (a) Normalized emission spectra and (b) photoluminescence decay profile of **4** in solid state at different temperatures of 77 K and 300 K upon excitation at 340 nm.

Table S2. Luminescence lifetimes of **1** in the solid state at different temperatures between 77 K and 300 K.

Temperature (T / K)	Lifetime 1 (τ_1 / μs)	Lifetime 2 (τ_1' / μs)	τ_1 %[a]	τ_1' %[a]
80	509	67.8	63.6	36.4
90	474	65.6	64.0	36.0
110	287	43.1	65.7	34.3
130	175	33.3	65.5	34.5
140	146	28.0	47.2	52.8
160	135	24.9	26.0	74.0
180	112	21.7	20.0	80.0
200	70.0	19.0	17.1	82.9
210	64.4	18.9	15.9	84.1
220	62.3	18.3	15.1	84.9
230	61.7	17.5	14.4	85.6
240		17.9		
250		15.9		
260		14.6		
270		13.9		
280		12.5		
290		12.5		

[a] τ_1 % and τ_1' % were calculated from the amplitudes and decay constants of τ_1 and τ_1' respectively.

Table S3. Luminescence lifetimes of **2** in the solid state at different temperatures between 77 K and 300 K.

Temperature (T / K)	Lifetime 1 (τ_1 / μs)	Lifetime 2 (τ_1' / μs)	τ_1 %[a]	τ_1' %[a]
77	5.1	36.2	79.7	20.3
100	3.9	13.4	67.4	32.6
200	1.1	3.6	64.0	36.0
300	0.6	2.0	59.1	40.9

[a] τ_1 % and τ_1' % were calculated from the amplitudes and decay constants of τ_1 and τ_1' respectively.

Table S4. Luminescence lifetimes of **3** in the solid state at different temperatures between 77 K and 300 K.

Temperature (T / K)	Lifetime 1 (τ_1 / μs)	Lifetime 2 (τ_1' / μs)	τ_1 %[a]	τ_1' %[a]
77	9.4	43.6	37.6	62.4
100	5.1	22.0	26.0	74.0
200	1.1	4.6	20.5	79.5
300	0.3	1.1	19.1	80.9

[a] τ_1 % and τ_1' % were calculated from the amplitudes and decay constants of τ_1 and τ_1' respectively.

Table S5. Luminescence lifetimes of **4** in the solid state at different temperatures of 77 K and 300 K.

Temperature (T / K)	Lifetime (τ / μs)
77	10.0
300	82.2

Computational studies

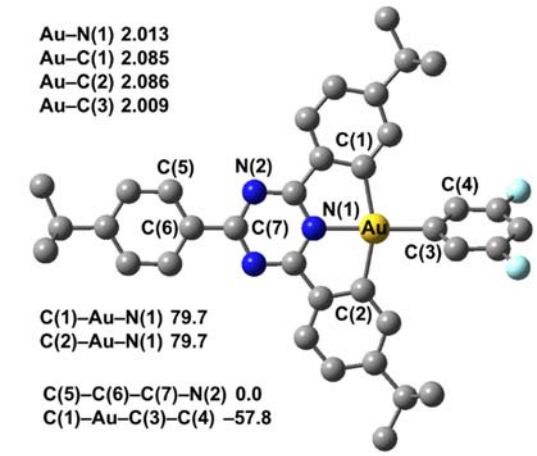

1

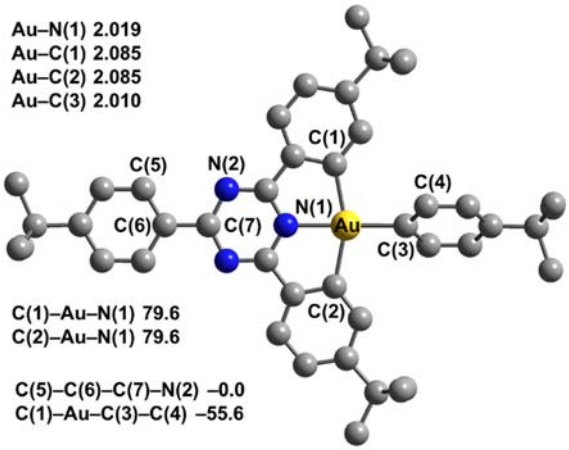

2

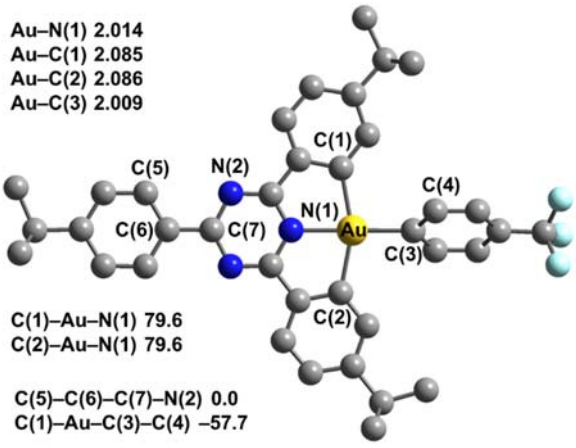

3

Figure S6. Selected structural parameters of the ground-state geometries of **1**−**3** obtained from the PBE0/CPCM (CH_2Cl_2) calculation.

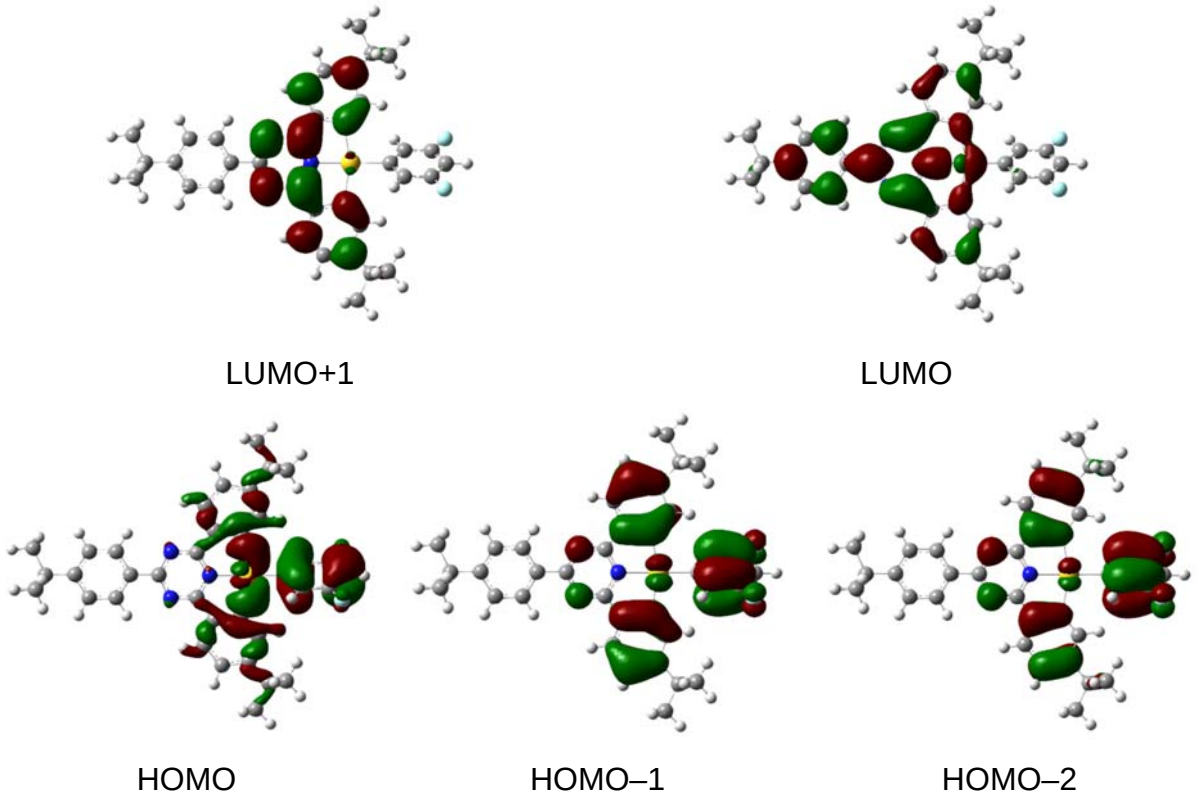

Figure S7. Spatial plots (isovalue = 0.03) of selected frontier molecular orbitals of **1** obtained from the PBE0/CPCM (CH_2Cl_2) calculation.

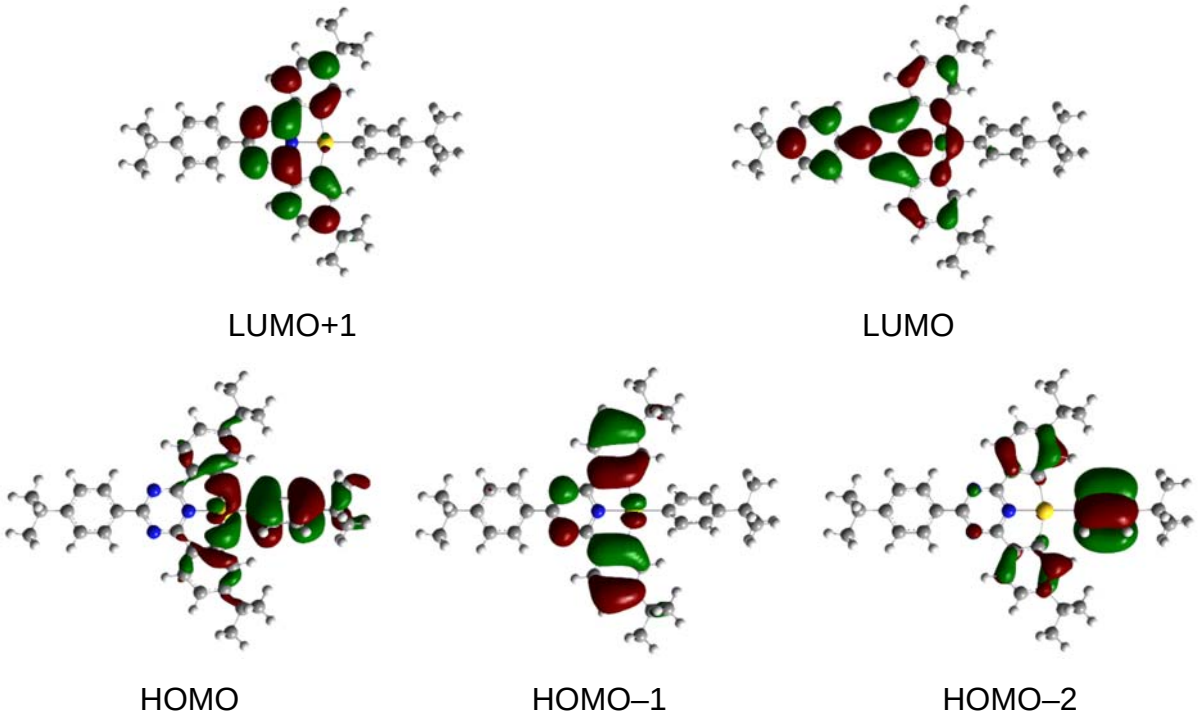

Figure S8. Spatial plots (isovalue = 0.03) of selected frontier molecular orbitals of **2** obtained from the PBE0/CPCM (CH_2Cl_2) calculation.

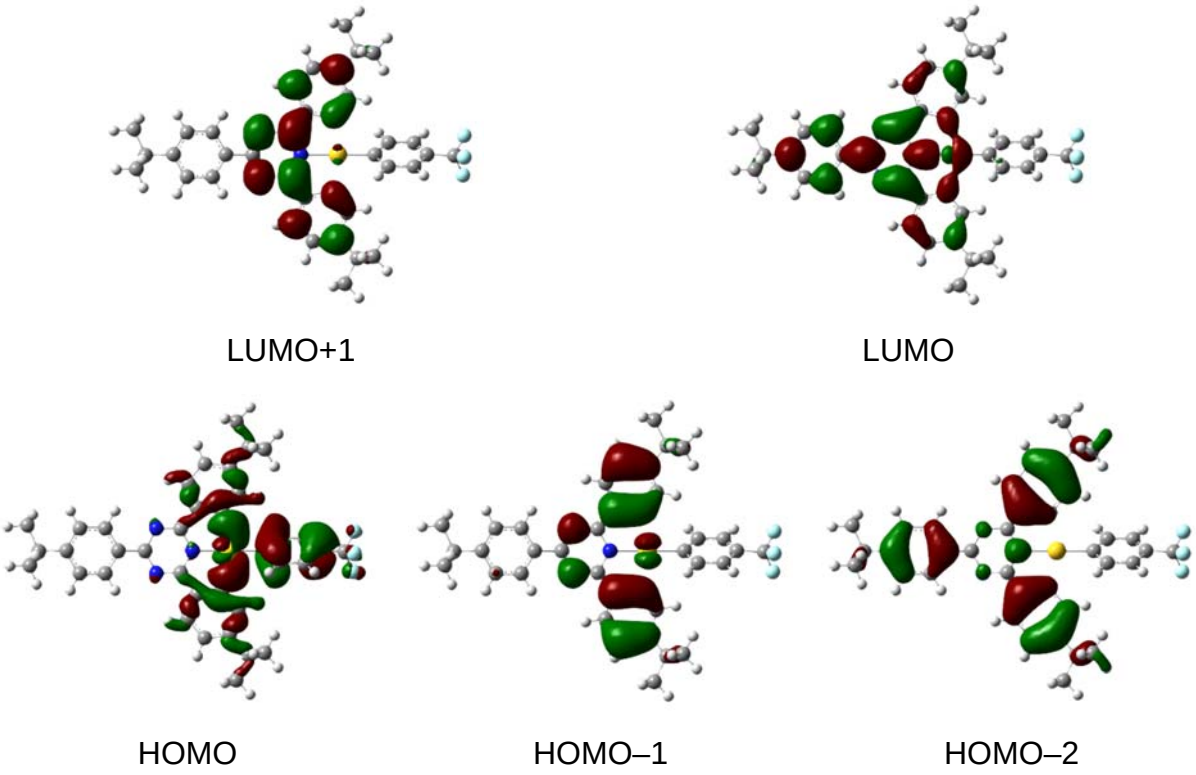

Figure S9. Spatial plots (isovalue = 0.03) of selected frontier molecular orbitals of **3** obtained from the PBE0/CPCM (CH_2Cl_2) calculation.

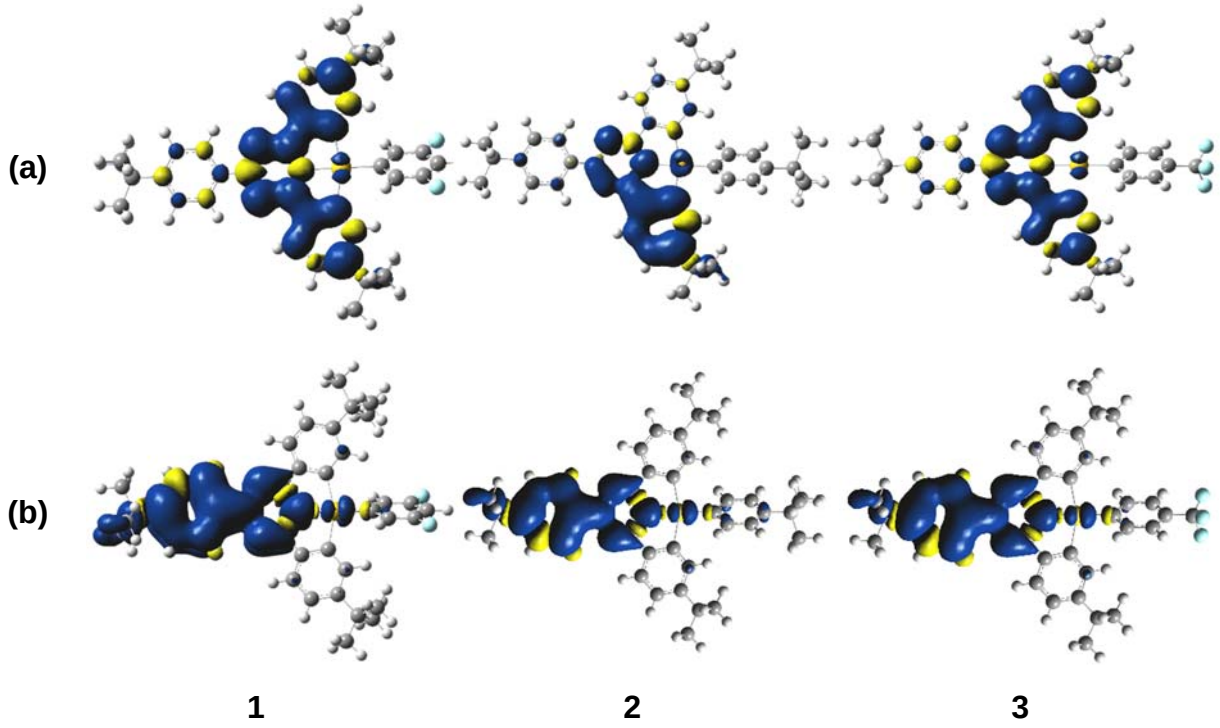

Figure S10. Plots of the spin density (isovalue = 0.002) of the (a) T_1' and (b) T_1 emissive states of **1**–**3** obtained from the PBE0/CPCM (CH_2Cl_2) calculation.

Table S6. The first ten singlet (S_n) excited states of **1**–**4** computed by TDDFT/CPCM (CH_2Cl_2) at the optimized ground-state geometries.

Complex	S_n	Excitation[a] (Coefficient)[b]	Vertical excitation wavelength / nm	f[c]	Character[d]
1	S_1	H → L (0.68)	367	0.014	LLCT
	S_2	H–1 → L (0.52)	352	0.035	LLCT/IL
		H–2 → L (0.46)	352	0.035	LLCT/IL
	S_3	H → L+1 (0.68)	339	0.001	LLCT
	S_4	H–5 → L (0.49)	324	0.079	ILCT
		H–2 → L (–0.31)			LLCT/IL
		H–1 → L (0.31)			LLCT/IL
	S_5	H–3 → L (0.69)	322	0.479	ILCT/IL
	S_6	H–2 → L (0.37)	316	0.178	LLCT/IL
		H–4 → L (0.36)			IL
		H–5 → L (0.33)			ILCT
		H–1 → L (–0.31)			LLCT/IL
	S_7	H–4 → L (0.55)	316	0.626	IL
	S_8	H–1 → L+1 (0.44)	308	0.156	LLCT/IL
		H–6 → L (0.33)			LLCT/ILCT
	S_9	H–9 → L (0.69)	304	0.000	IL
	S_{10}	H–4 → L+1 (0.49)	301	0.490	ILCT/IL
		H–3 → L+1 (–0.41)			ILCT/IL
2	S_1	H → L (0.68)	389	0.034	LLCT
	S_2	H → L+1 (0.67)	357	0.000	LLCT
	S_3	H–1 → L (0.68)	351	0.032	ILCT
	S_4	H–5 → L (0.52)			LLCT/ILCT
		H–2 → L (–0.37)	322	0.087	LLCT
	S_5	H–3 → L (0.67)	321	0.204	LLCT
	S_6	H–4 → L (0.52)			IL
		H–6 → L (–0.37)	319	0.615	LLCT
	S_7	H–6 → L (0.47)			LLCT
		H–4 → L (0.39)	312	0.494	IL
	S_8	H–1 → L+1 (0.50)	309	0.123	ILCT/IL
		H–7 → L (0.34)			ILCT
	S_9	H–2 → L (0.55)	308	0.026	LLCT
		H–5 → L (0.30)			LLCT/ILCT
	S_{10}	H–10 → L (0.69)	302	0.000	IL
3	S_1	H → L (0.69)	367	0.015	LLCT/IL
	S_2	H–1 → L (0.69)	352	0.034	ILCT
	S_3	H → L+1 (0.69)	339	0.001	LLCT
	S_4	H–2 → L (0.56)	322	0.337	ILCT/IL
		H–4 → L (0.35)			ILCT
	S_5	H–4 → L (0.52)	322	0.217	ILCT
		H–2 → L (–0.40)			ILCT/IL
	S_6	H–3 → L (0.64)	316	0.829	IL

	S_7	H–1 → L+1 (0.50)	308	0.155	IL
		H–5 → L (0.36)			LLCT/ILCT
	S_8	H–9 → L (0.69)	303	0.000	ILCT/IL
	S_9	H–3 → L+1 (0.48)	301	0.494	ILCT/IL
		H–2 → L+1 (–0.42)			ILCT/IL
	S_{10}	H–7 → L (0.66)	298	0.013	ILCT/IL
4	S_1	H → L (0.68)	351	0.006	LLCT
	S_2	H → L+1 (0.67)	338	0.001	LLCT
	S_3	H–1 → L (0.51)	335	0.053	LLCT/ILCT
		H–2 → L (–0.41)			LLCT/ILCT
	S_4	H–4 → L (0.46)	310	0.022	ILCT
	S_5	H–1 → L+1 (0.44)	309	0.078	LLCT/IL
		H–3 → L (–0.36)			ILCT
	S_6	H–2 → L (0.46)	302	0.052	LLCT/ILCT
		H–1 → L (0.39)			LLCT/ILCT
	S_7	H–3 → L (0.52)	300	0.17	LLCT/IL
	S_8	H–3 → L+1 (0.57)	296	0.59	ILCT/IL
		H–4 → L (–0.36)			ILCT
	S_9	H–2 → L+1 (0.61)	293	0.023	LLCT/IL
		H–1 → L+1 (0.32)			LLCT/IL
	S_{10}	H–7 → L (0.68)	291	0.000	IL
		H–1 → L+1 (0.32)			LLCT/IL

[a] The orbitals involved in the excitation (H = HOMO and L = LUMO). [b] The coefficients in the configuration interaction (CI) expansion that are less than 0.3 are not listed. [c] Oscillator strengths. [d] Character of the transition.

Mechanochromic studies

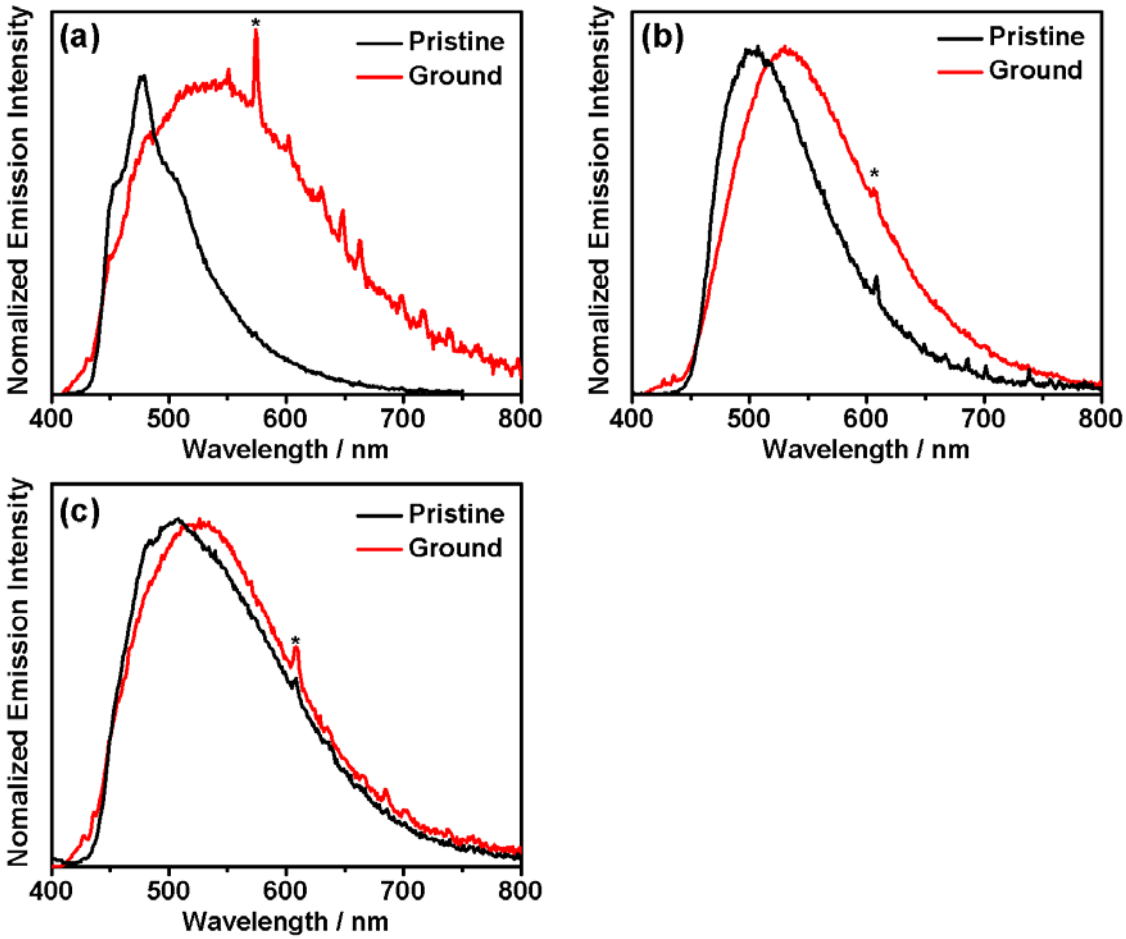

Figure S11. Normalized emission spectra of (a) **1**, (b) **2** and (c) **3** in pristine and ground solid-state forms (the asterisk indicates an instrumental artifact).

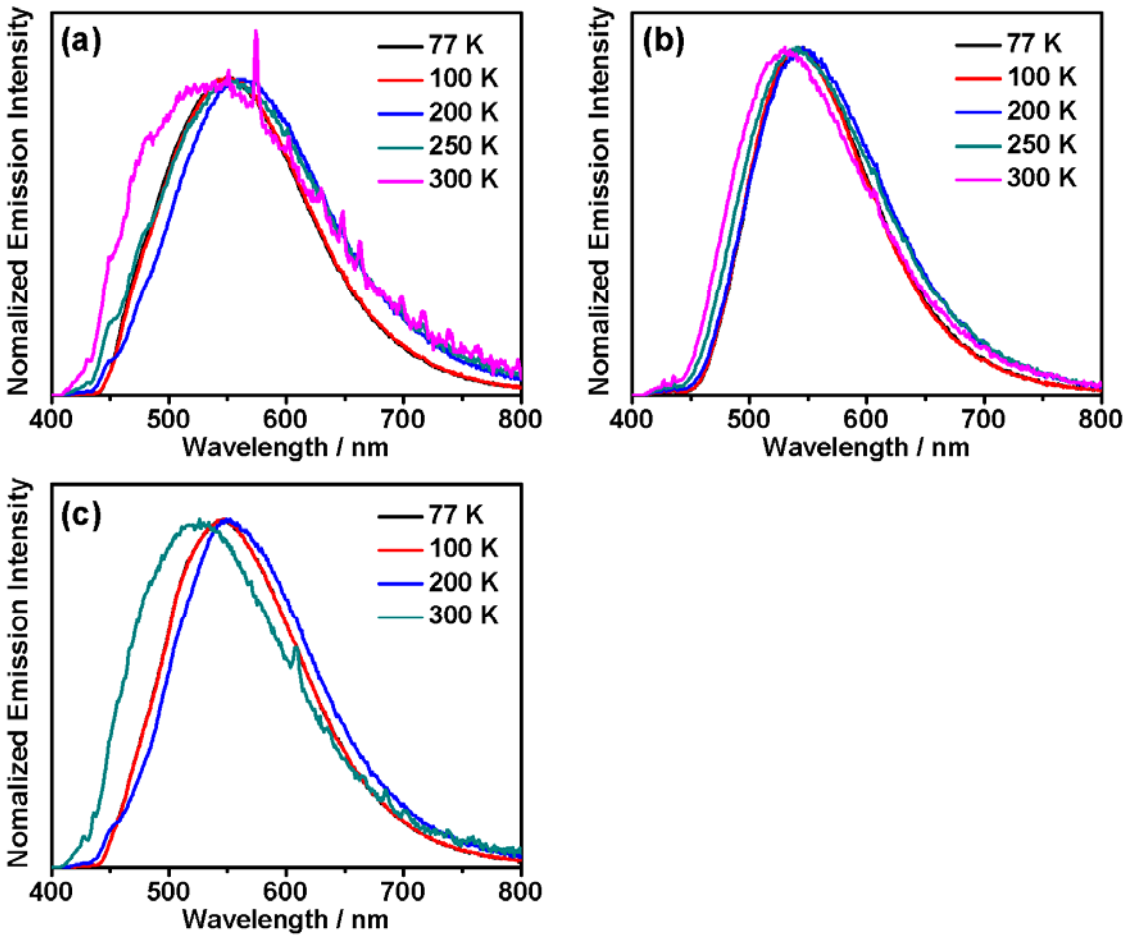

Figure S12. Normalized ground solid-state emission spectra of (a) **1**, (b) **2** and (c) **3** at different temperatures between 77 K and 300 K upon excitation at 360 nm.

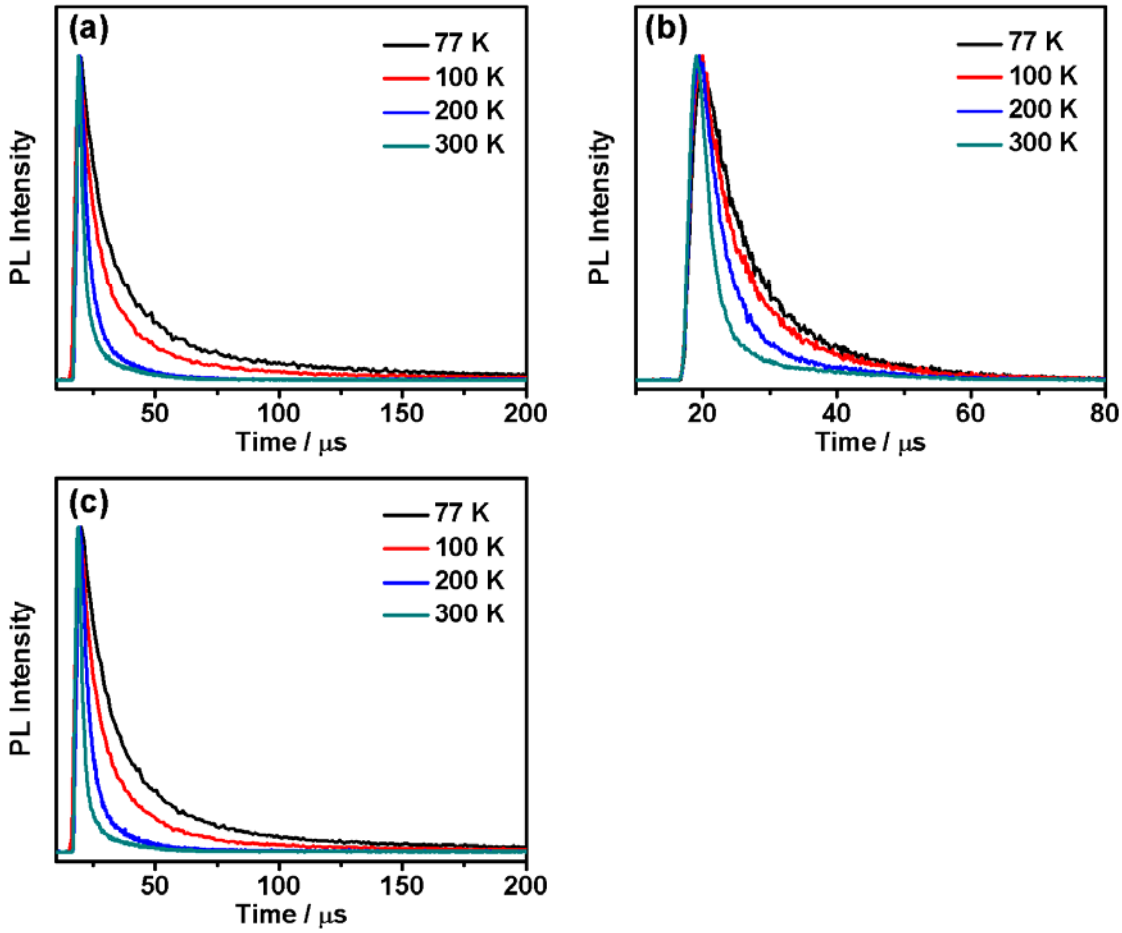

Figure S13. Photoluminescence decay profile of (a) **1**, (b) **2** and (c) **3** in ground solid-state at different temperatures between 77 K and 300 K upon excitation at 340 nm.

Table S7. Luminescence lifetimes of **1** in ground solid-state at different temperatures between 77 K and 300 K.

Temperature (T / K)	Lifetime 1 (τ_1 / μs)	Lifetime 2 (τ_1' / μs)	τ_1 %[a]	τ_1' %[a]
77	139	41.0	81.4	18.6
100	112	28.8	79.8	20.2
200	38.4	11.6	42.9	57.1
300	10.6	2.2	39.5	60.5

[a] τ_1 % and τ_1' % were calculated from the amplitudes and decay constants of τ_1 and τ_1' respectively.

Table S8. Luminescence lifetimes of **2** in ground solid-state at different temperatures between 77 K and 300 K.

Temperature (T / K)	Lifetime 1 (τ_1 / μs)	Lifetime 2 (τ_1' / μs)	τ_1 %[a]	τ_1' %[a]
77	8.0			
100	6.4			
200	10.8	2.7	73.5	26.5
300	2.7	1.2	32.7	67.3

[a] τ_1 % and τ_1' % were calculated from the amplitudes and decay constants of τ_1 and τ_1' respectively.

Table S9. Luminescence lifetimes of **3** in ground solid-state at different temperatures between 77 K and 300 K.

Temperature (T / K)	Lifetime 1 (τ_1 / μs)	Lifetime 2 (τ_1' / μs)	τ_1 %[a]	τ_1' %[a]
77	56.2	241	36.7	63.3
100	26.0	189	38.5	61.5
200	11.9	147	57.3	42.7
300	2.2	12.2	15.5	84.5

[a] τ_1 % and τ_1' % were calculated from the amplitudes and decay constants of τ_1 and τ_1' respectively.

X-Ray crystal structure

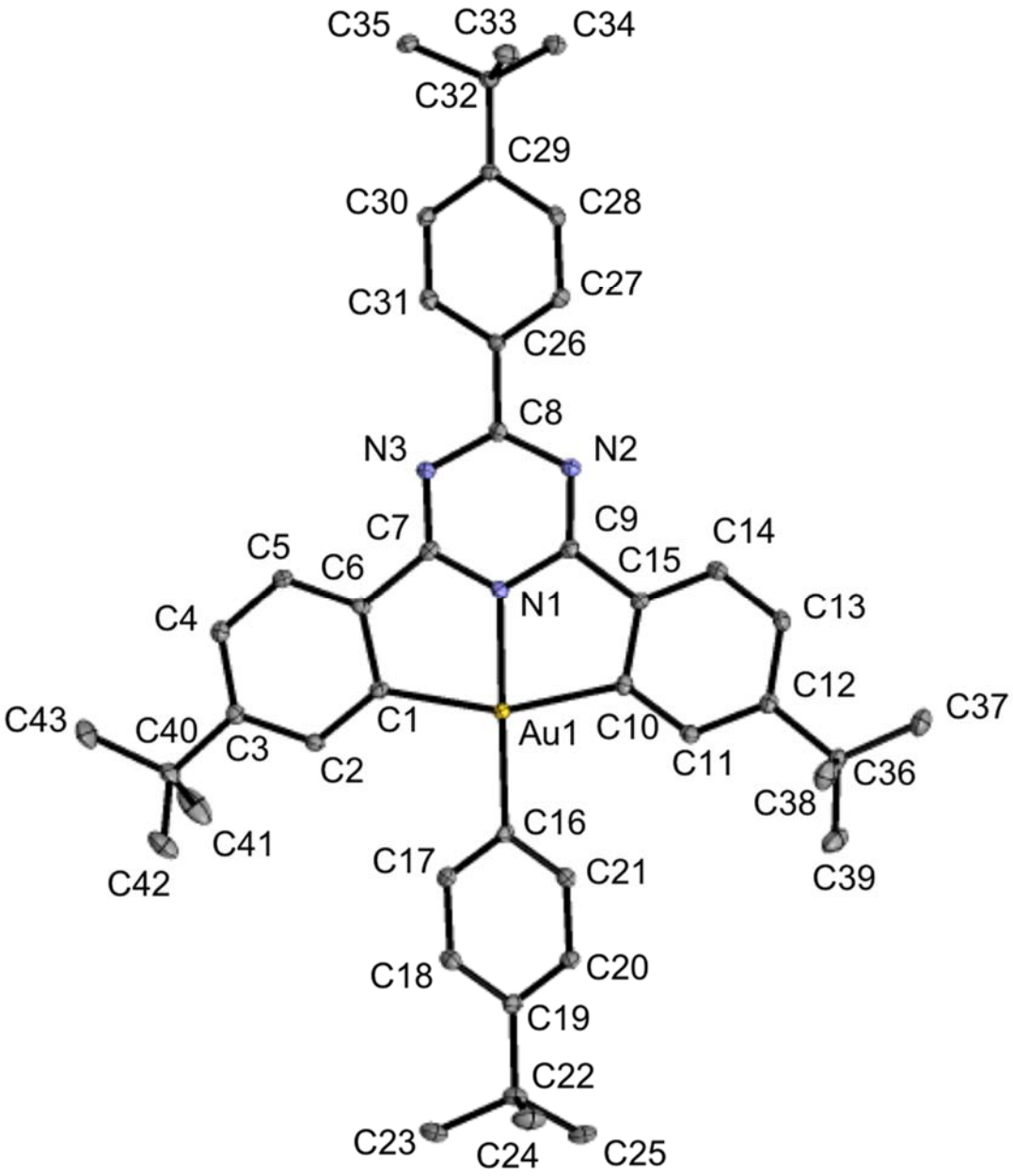

Figure S14. Perspective view of **2** with an atomic numbering scheme. The hydrogen atoms have been omitted for clarity. The thermal ellipsoids are drawn at the 30 % probability level.

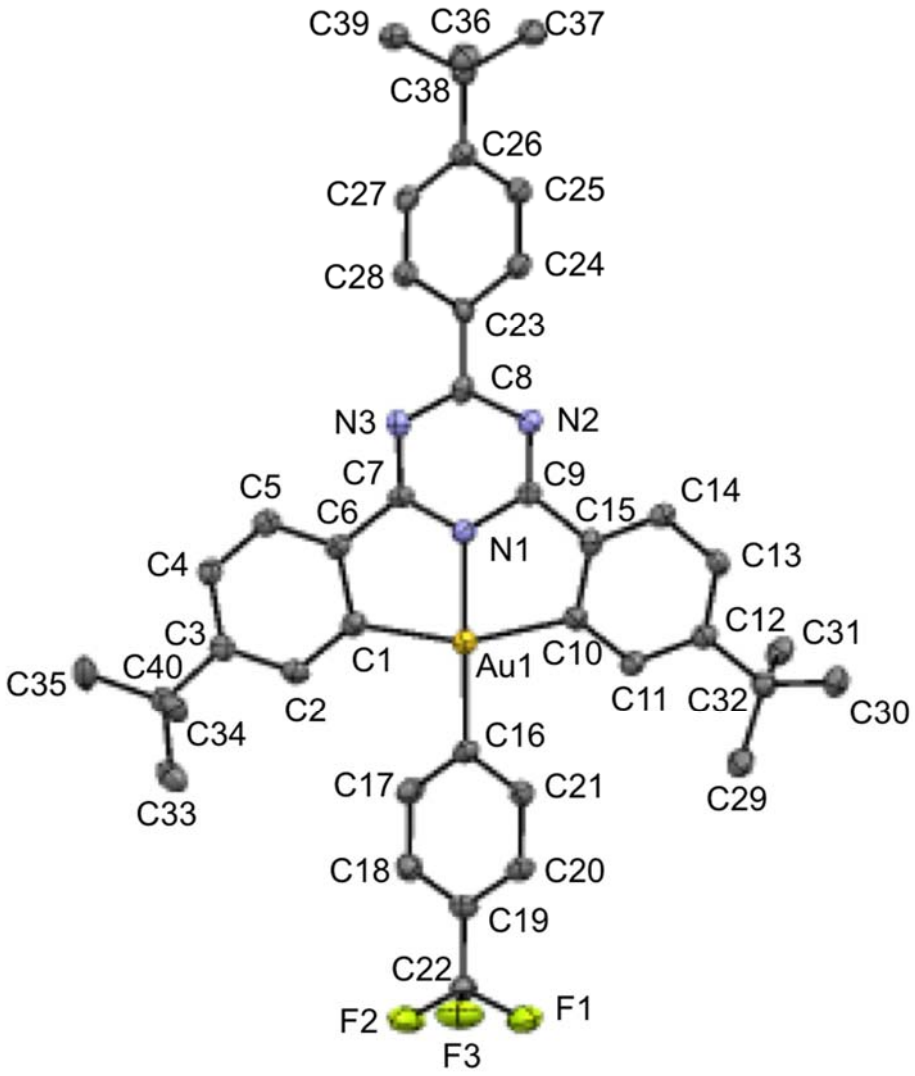

Figure S15. Perspective view of **3** with an atomic numbering scheme. The hydrogen atoms and the solvent molecule have been omitted for clarity. The thermal ellipsoids are drawn at the 30 % probability level.

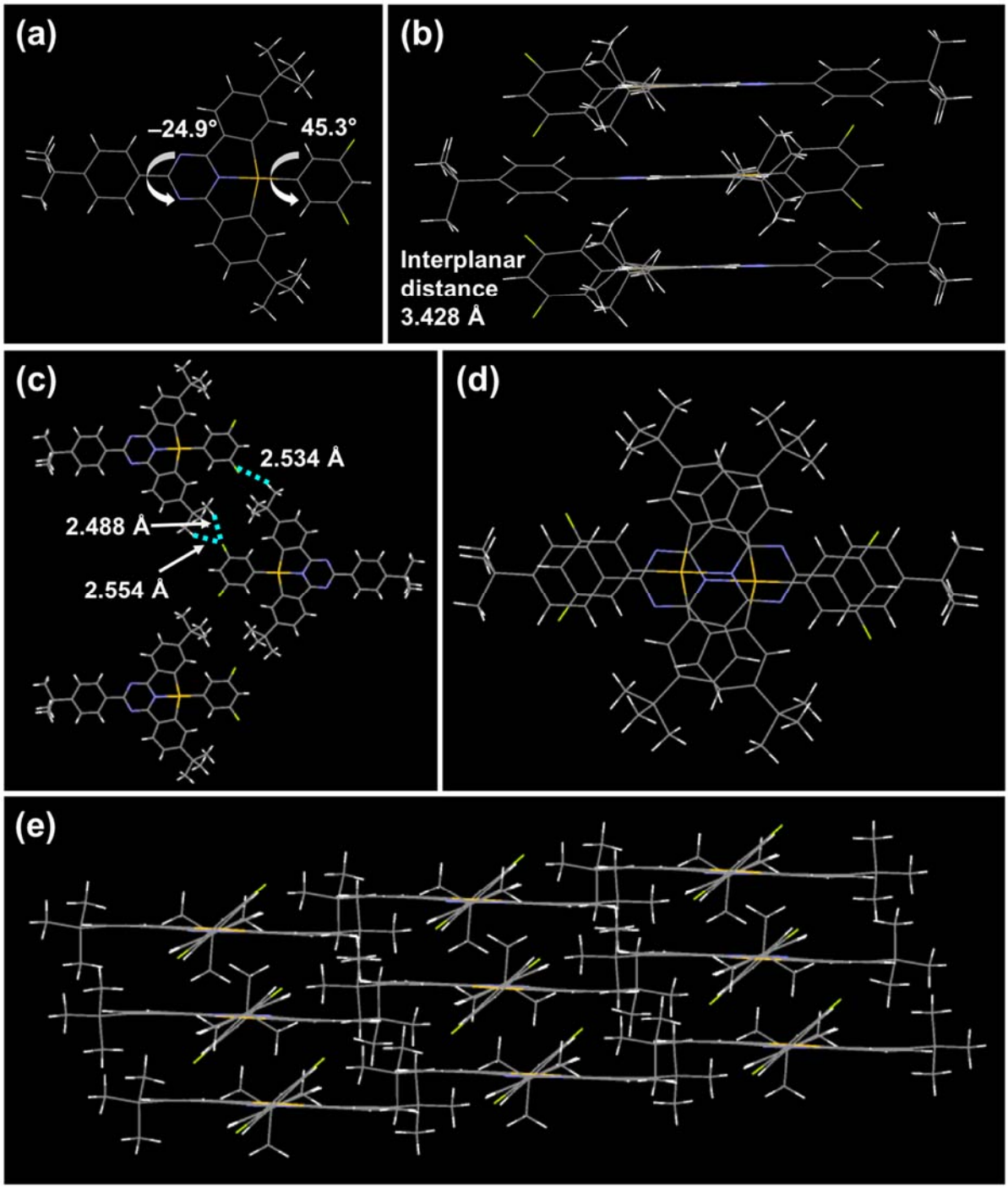

Figure S16. Single crystal structure of **1**: (a) molecular structure, (b) molecular packing mode, (c) intermolecular interactions, (d) packing viewed along a-axis and (e) packing viewed along b-axis.

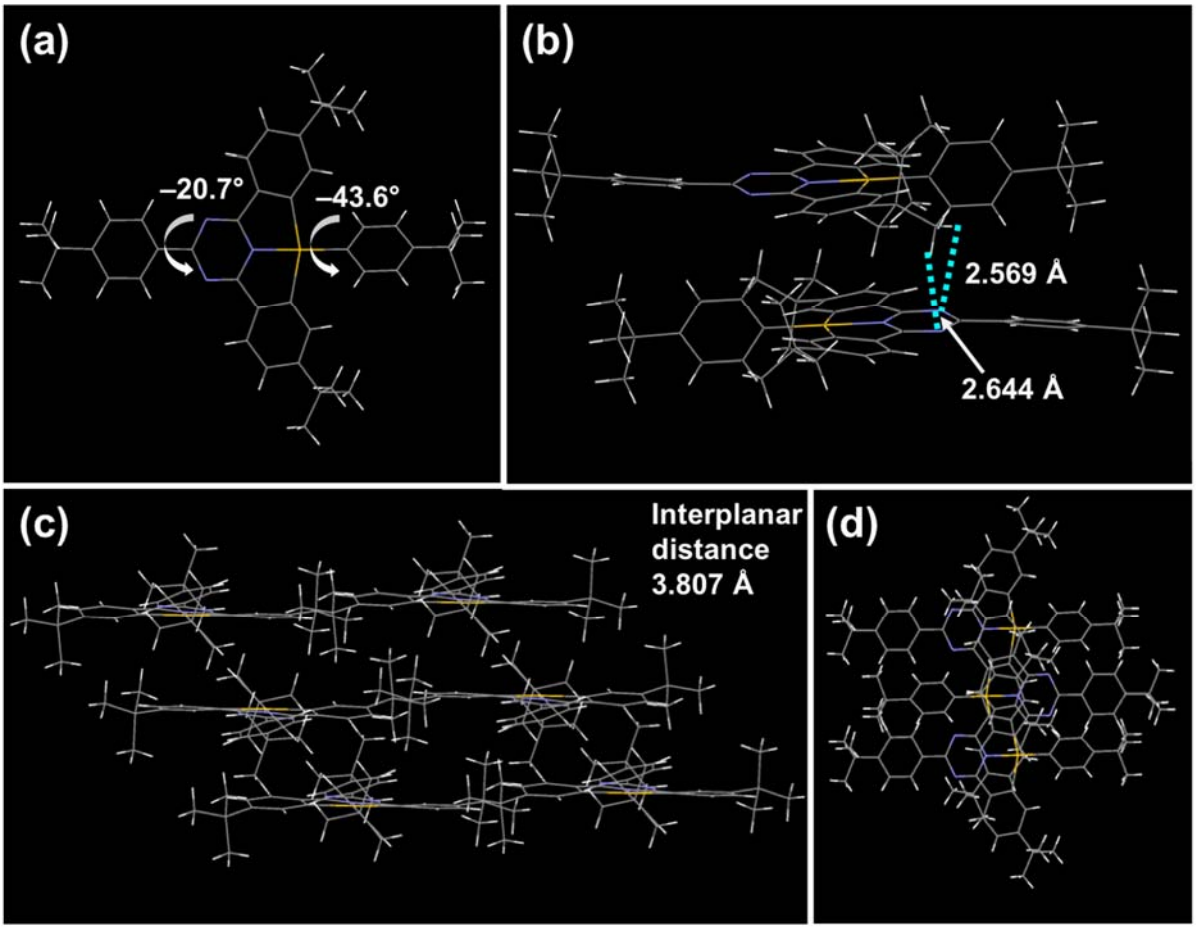

Figure S17. Single crystal structure of **2**: (a) molecular structure, (b) intermolecular interactions and (c, d) molecular packing mode.

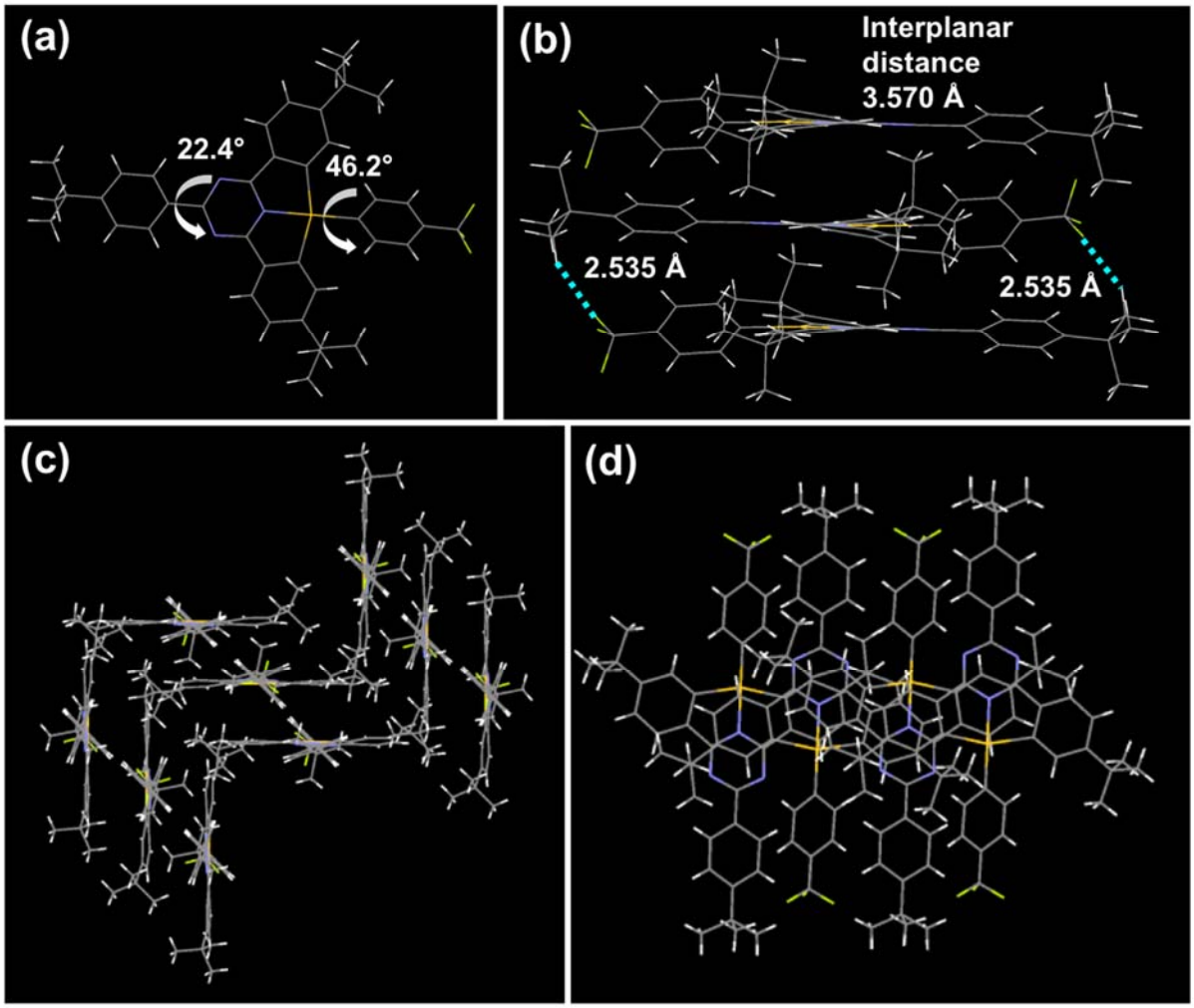

Figure S18. Single crystal structure of **3**: (a) molecular structure, (b) intermolecular interactions and (c, d) molecular packing mode. The solvent molecules have been omitted for clarity.

Table S10. Crystal and structure determination data of **1**–**3**.

Complex	**1**	**2**	**3**
Empirical formula	$C_{39}H_{40}AuF_2N_3$	$C_{43}H_{50}AuN_3$	$C_{44}H_{51}AuF_3N_3O$
Formula weight	785.70	805.82	891.84
Temperature, K	100(2)	149(2)	100(2)
Wavelength, Å	0.71073	0.71073	0.71073
Crystal system	Monoclinic	Triclinic	Monoclinic
z	$P2_1/n$	P–1	$P2_1/c$
a, Å	7.3969(4)	10.6434(14)	17.1108(8)
b, Å	22.2469(11)	11.5563(14)	10.1518(5)
c, Å	20.6523(10)	15.779(2)	23.0061(11)
α, deg	90	101.439(3)	90
β, deg	98.4420(10)	98.369(4)	94.888(2)
γ, deg	90	104.009(3)	90
Volume, $Å^3$	3361.7(3)	1807.1(4)	3981.8(3)
Z	4	2	4
Density (calcd), g cm^{-3}	1.552	1.481	1.488
F_{000}	1568.0	816.0	1800.0
2θ range for data collection, deg	4.17 to 50.052	4.028 to 50.076	4.388 to 50.146
Index ranges	$-8 \le h \le 8$	$-12 \le h \le 12$	$-20 \le h \le 20$
	$-26 \le k \le 26$	$-13 \le k \le 13$	$-11 \le k \le 12$
	$-24 \le l \le 24$	$-18 \le l \le 18$	$-27 \le l \le 27$
Reflections collected (unique)	25210	62245	42326
Goodness-of-fit on F^2	1.036	1.067	1.055
Final R indices [I > σ2(I)]	$R_1 = 0.0277$,	$R_1 = 0.0215$,	$R_1 = 0.0495$,
	$wR_2 = 0.0684$	$wR_2 = 0.0426$	$wR_2 = 0.1075$
Largest diff. peak and hole e $Å^{-3}$	1.82 and –1.33	0.60 and –1.03	1.78 and –0.67

Table S11. Selected bond distances (Å), bond angles (°) and torsion angles (°) of **1** with estimated deviations (esds) in parentheses.

Bond distances (Å)	
Au–N(1)	2.008(3)
Au–C(10)	2.085(4)
Au–C(1)	2.086(4)
Au–C(16)	2.003(4)

Bond angles (°)	
C(10)–Au–N(1)	79.45(12)
C(1)–Au–N(1)	79.47(12)
C(16)–Au–C(10)	100.52(13)
C(1)–Au–C(16)	100.56(13)

Bond torsions (°)	
C(23)–C(22)–C(8)–N(2)	–24.9(5)
C(1)–Au–C(16)–C(17)	45.3(3)

Table S12. Selected bond distances (Å), bond angles (°) and torsion angles (°) of **2** with estimated deviations (esds) in parentheses.

Bond distances (Å)	
Au–N(1)	2.015(2)
Au–C(1)	2.094(3)
Au–C(10)	2.093(3)
Au–C(16)	2.021(3)

Bond angles (°)	
C(1)–Au–N(1)	79.36(10)
C(10)–Au–N(1)	79.05(10)
C(1)–Au–C(16)	100.00(11)
C(10)–Au–C(16)	101.59(11)

Bond torsions (°)	
C(32)–C(27)–C(8)–N(2)	–20.7(5)
C(1)–Au–C(16)–C(17)	–43.6(3)

Table S13. Selected bond distances (Å), bond angles (°) and torsion angles (°) of **3** with estimated deviations (esds) in parentheses.

Bond distances (Å)	
Au–N(1)	2.010(5)
Au–C(1)	2.084(7)
Au–C(10)	2.092(6)
Au–C(15)	2.006(7)

Bond angles (°)	
C(1)–Au–N(1)	79.7(2)
C(10)–Au–N(1)	79.5(2)
C(15)–Au–C(1)	100.1(3)
C(15)–Au–C(10)	100.6(3)

Bond torsions (°)	
C(24)–C(23)–C(8)–N(2)	22.4(9)
C(1)–Au–C(15)–C(21)	46.2(6)

Solid-state thin film studies

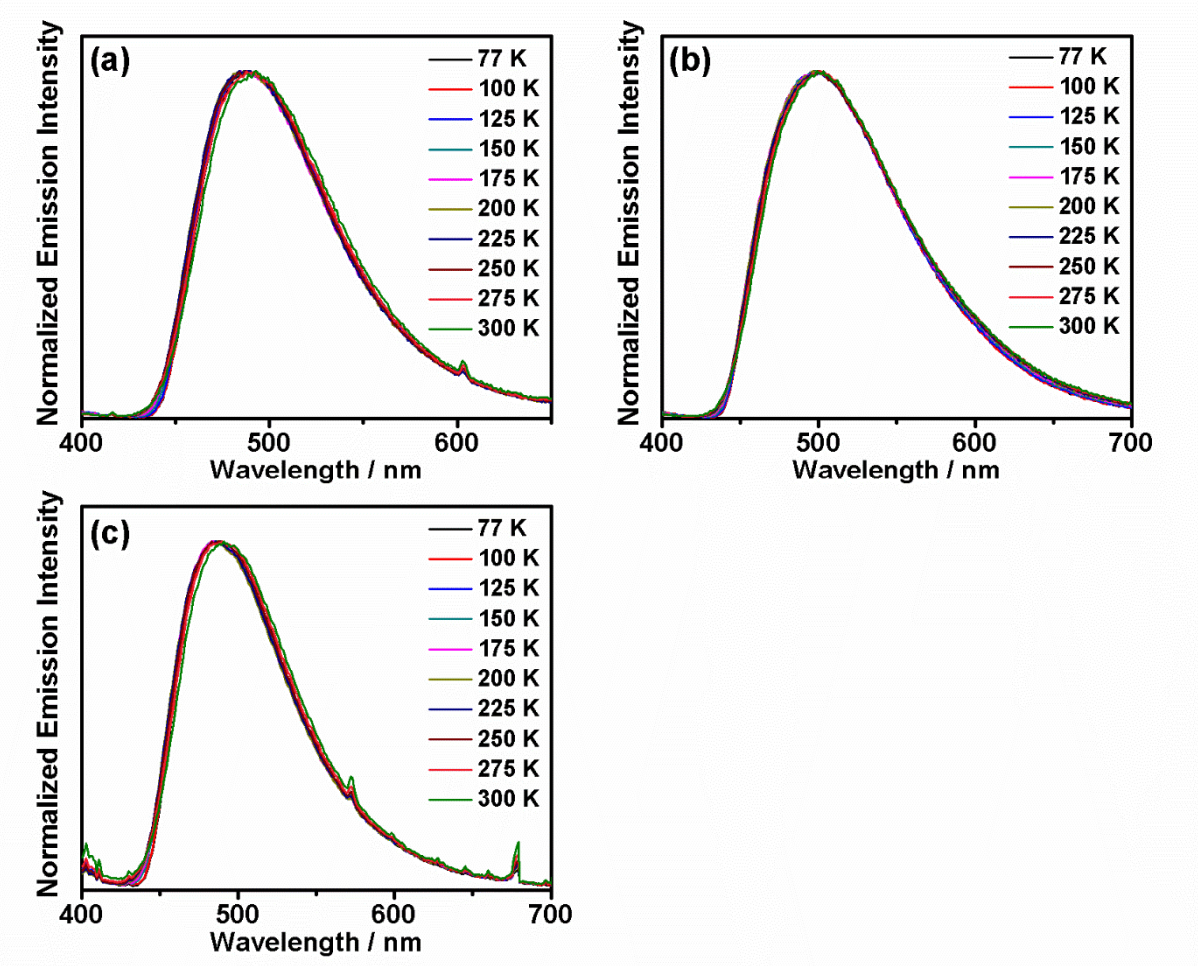

Figure S19. Normalized photoluminescence spectra of vacuum-deposited thin films of (a) **1**, (b) **2** and (c) **3** doped into PYD-2Cz at 10 wt% at different temperatures between 77 K and 300 K upon excitation at 340 nm.

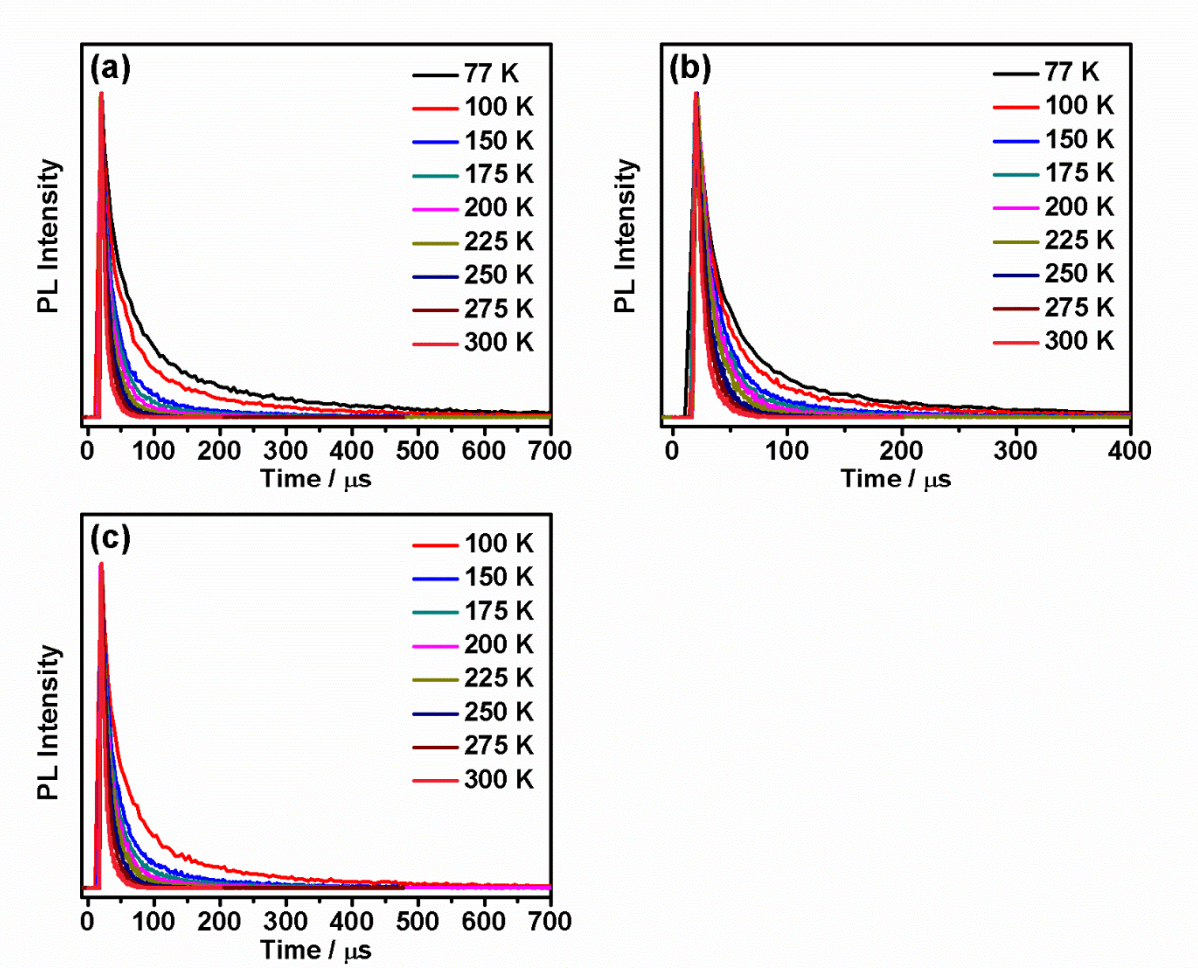

Figure S20. Photoluminescence decay profile of (a) **1**, (b) **2** and (c) **3** doped into PYD-2Cz at 10 wt% in vacuum-deposited thin films at different temperatures between 77 K and 300 K upon excitation at 340 nm.

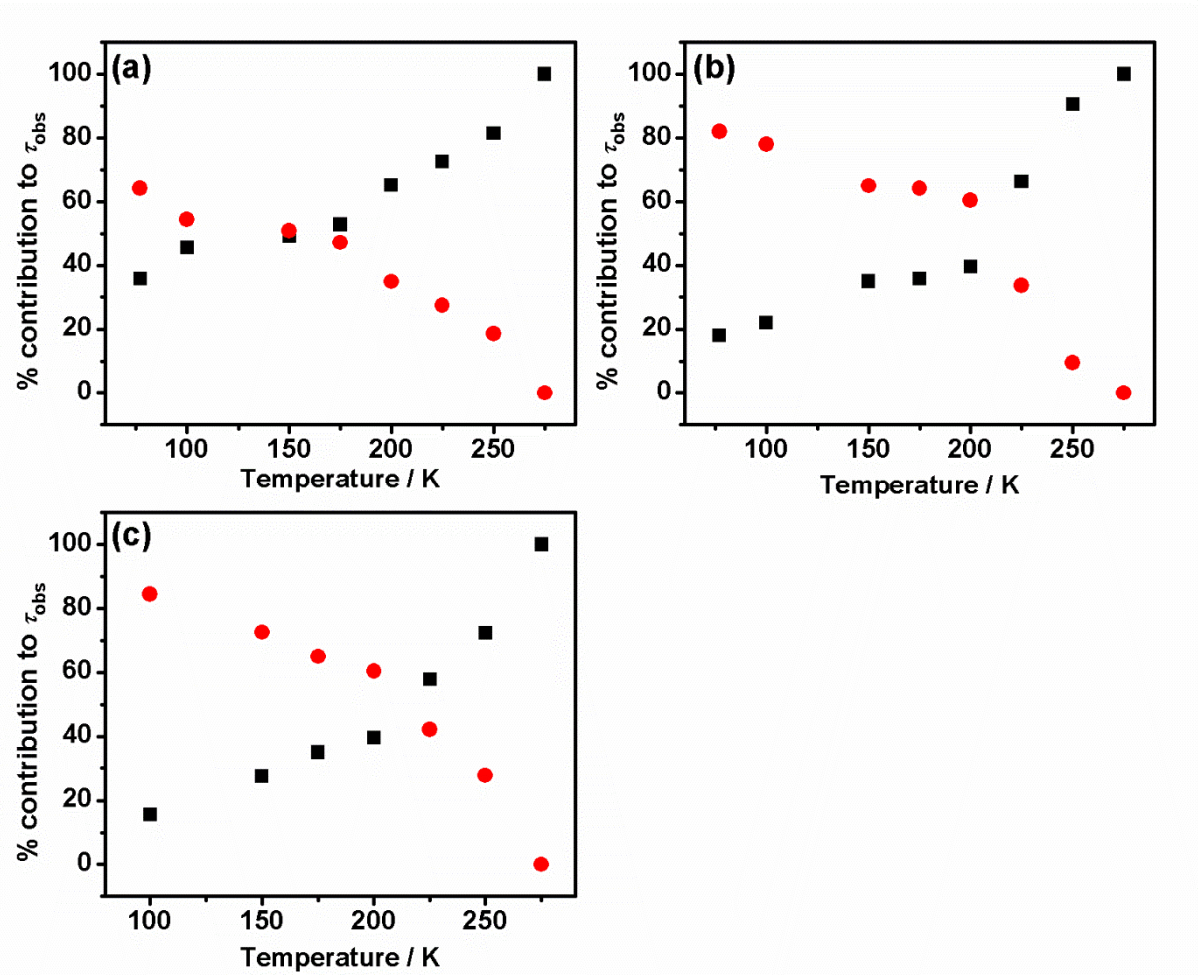

Figure S21. Plots of percentage contribution of τ_1 and τ_1' to apparent lifetimes (τ_{obs}) against temperature of (a) **1**, (b) **2** and (c) **3** doped into PYD-2Cz at 10 wt% in vacuum-deposited thin films (● = τ_1, ■ = τ_1').

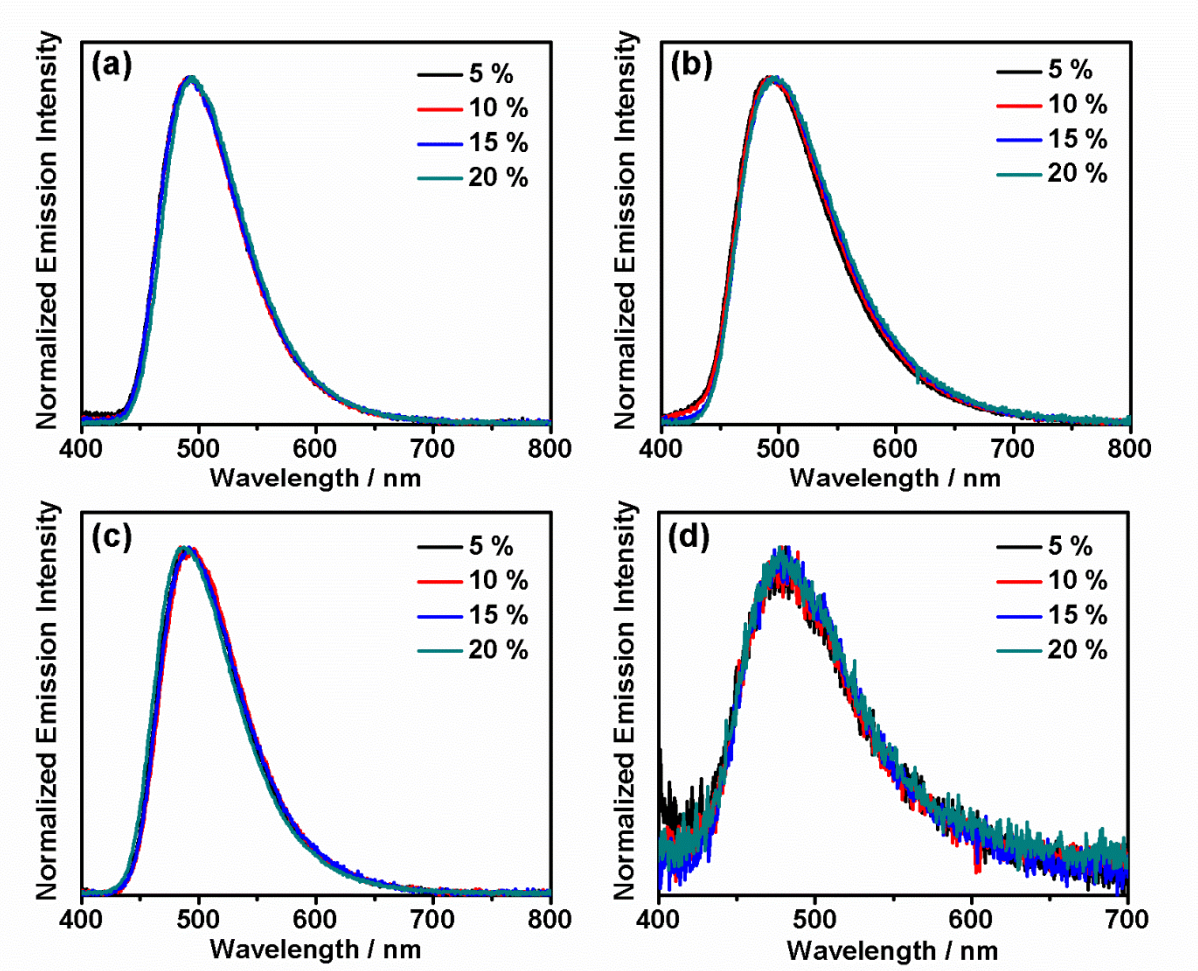

Figure S22. Normalized photoluminescence spectra of solution-processed thin films of (a) **1**, (b) **2** (c) **3** and (d) **4** doped into MCP at different concentrations (wt%) at 298 K.

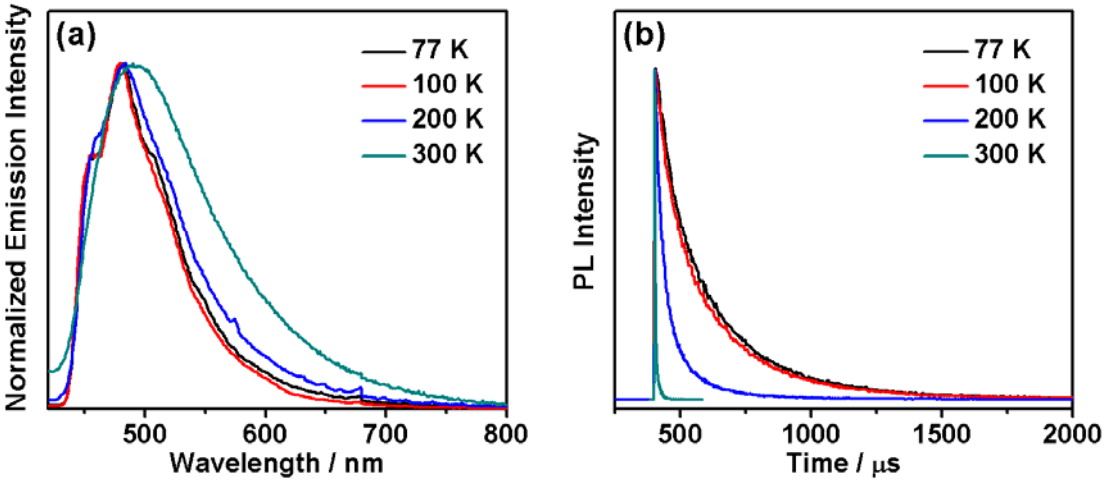

Figure S23. (a) Normalized photoluminescence spectra and (b) photoluminescence decay profile of solution-processed thin films of **4** doped into MCP at 10 wt% at different temperatures between 77 K and 300 K upon excitation at 340 nm.

Table S14. Luminescence lifetimes of vacuum-deposited thin films of **1** doped into PYD-2Cz at 10 wt% at different temperatures between 77 K and 300 K.

Temperature (T / K)	Lifetime 1 (τ_1 / μs)	Lifetime 2 (τ_1' / μs)	τ_1 %[a]	τ_1' %[a]
77	321	71.7	64.1	35.9
100	303	81.4	54.4	45.6
150	136	27.7	50.9	49.1
175	100	21.5	47.1	52.9
200	73.8	17.6	34.9	65.1
225	53.1	15.4	27.5	72.5
250	36.7	12.6	18.6	81.4
275		12.0		
300		11.0		

[a] τ_1 % and τ_1' % were calculated from the amplitudes and decay constants of τ_1 and τ_1' respectively.

Table S15. Luminescence lifetimes of vacuum-deposited thin films of **2** doped into PYD-2Cz at 10 wt% at different temperatures between 77 K and 300 K.

Temperature (T / K)	Lifetime 1 (τ_1 / μs)	Lifetime 2 (τ_1' / μs)	τ_1 %[a]	τ_1' %[a]
77	301	88.0	82.0	18.0
100	243	71.8	78.0	22.0
150	124	32.3	65.0	35.0
175	73.0	18.8	64.2	35.8
200	55.3	14.9	60.4	39.6
225	46.0	14.1	33.7	66.3
250	42.1	13.4	9.4	90.6
275		11.7		
300		11.1		

[a] τ_1 % and τ_1' % were calculated from the amplitudes and decay constants of τ_1 and τ_1' respectively.

Table S16. Luminescence lifetimes of vacuum-deposited thin films of **3** doped into PYD-2Cz at 10 wt% at different temperatures between 77 K and 300 K.

Temperature (T / K)	Lifetime 1 (τ_1 / μs)	Lifetime 2 (τ_1' / μs)	τ_1 %[a]	τ_1' %[a]
100	334	109	84.5	15.5
150	164	48.1	72.5	27.5
175	106	25.8	65.0	35.0
200	77.6	19.2	60.4	39.6
225	70.0	17.8	42.2	57.8
250	65.7	14.5	27.8	72.2
275		12.1		
300		11.0		

[a] τ_1 % and τ_1' % were calculated from the amplitudes and decay constants of τ_1 and τ_1' respectively.

Table S17. Luminescence lifetimes of vacuum-deposited thin films of **4** doped into MCP at 10 wt% at different temperatures between 77 K and 300 K.

Temperature (T / K)	Lifetime (τ_1 / μs)
77	360
100	335
200	178
300	10.9

Electroluminescence studies

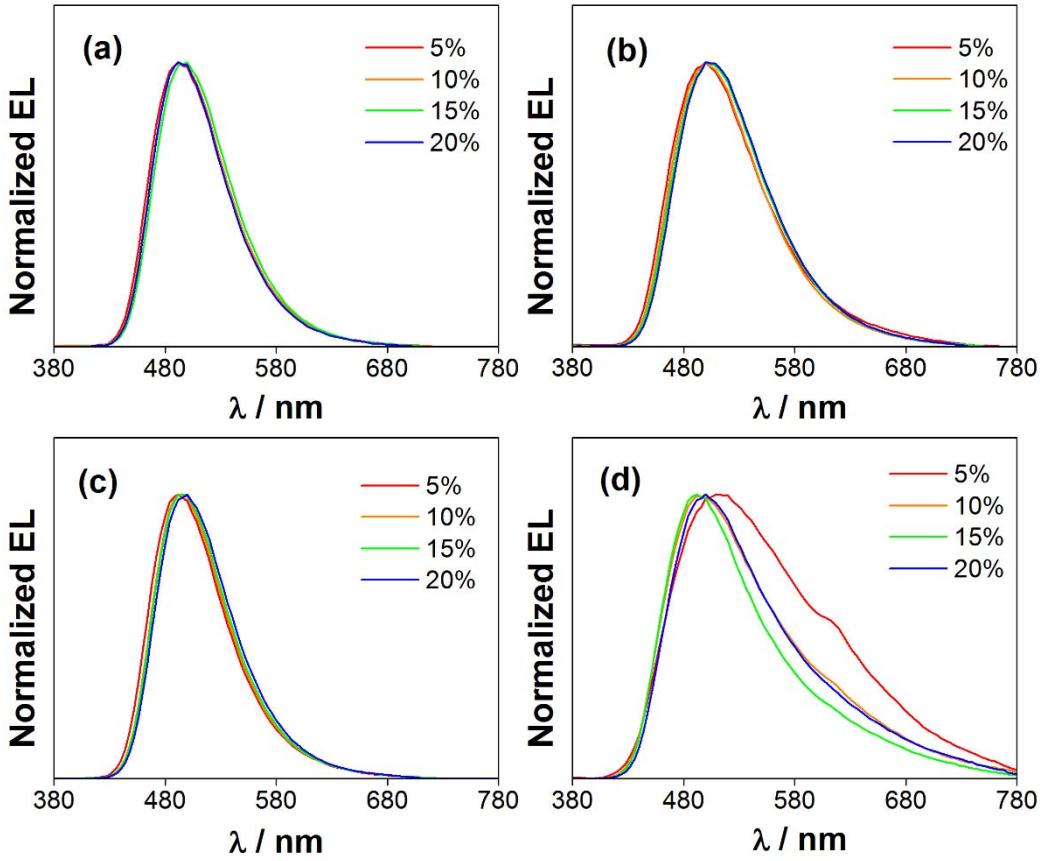

Figure S24. Normalized EL spectra of the solution-processed OLEDs based on **1**–**4**.

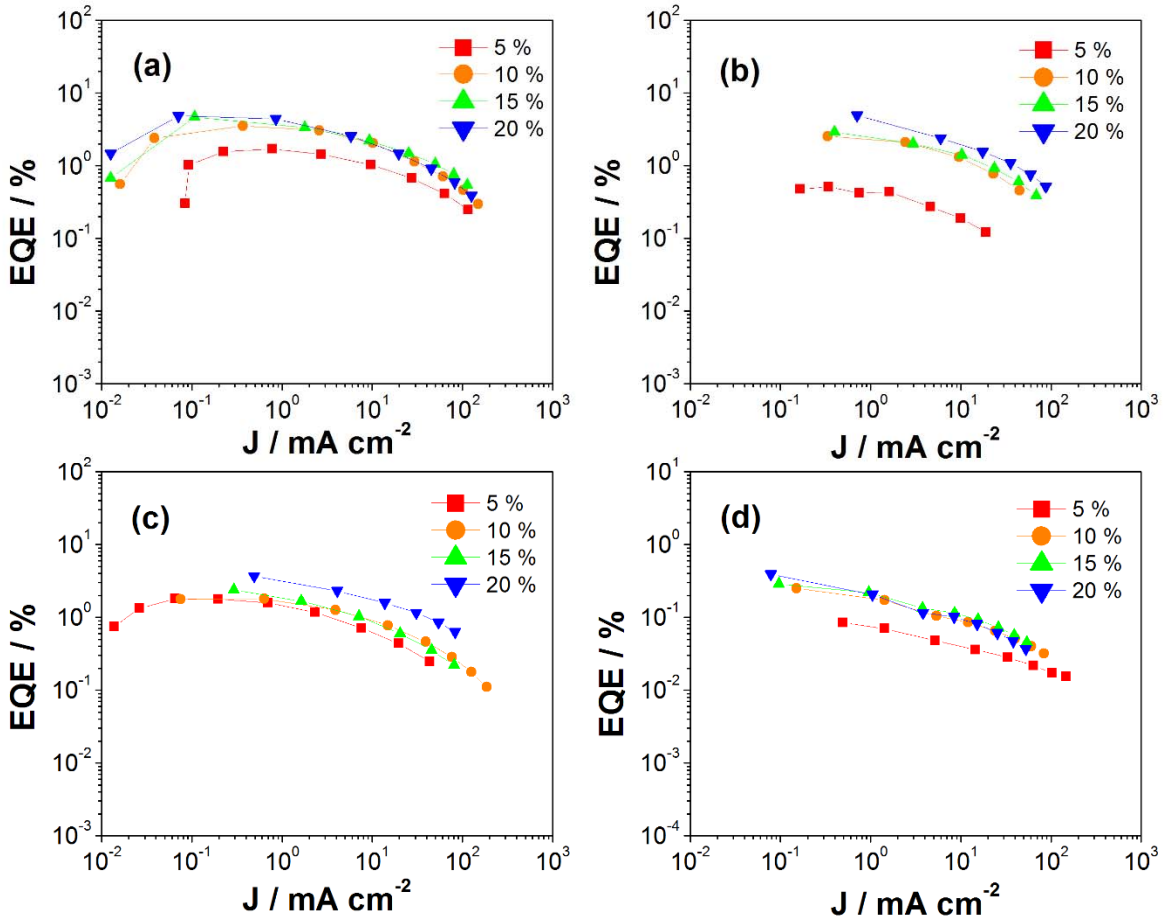

Figure S25. EQEs of the solution-processed OLEDs based on **1**–**4**.

Table S18. Key parameters of the solution-processable devices based on **1**–**4**.

Complex	Dopant conc. / wt %	Max. current efficiency / cd A^{-1}	Max. power efficiency / lm W^{-1}	Max. EQE / %	λ_{max} / nm	CIE (x, y)[a]
1	5	4.2	1.5	1.7	492	0.19, 0.41
	10	8.9	4.0	3.6	492	0.20, 0.43
	15	12.2	6.4	4.7	500	0.21, 0.46
	20	12.2	6.4	4.8	492	0.20, 0.43
2	5	1.2	0.4	0.5	500	0.24, 0.44
	10	6.8	2.7	2.5	500	0.24, 0.45
	15	7.9	3.1	2.9	500	0.24, 0.47
	20	13.6	6.1	4.9	500	0.25, 0.48
3	5	4.4	2.0	1.8	492	0.19, 0.41
	10	4.6	2.4	1.8	492	0.20, 0.44
	15	6.1	2.8	2.4	500	0.20, 0.44
	20	9.7	5.1	3.7	500	0.21, 0.46
4	5	0.2	0.1	0.1	512	0.33, 0.44
	10	0.6	0.3	0.3	500	0.28, 0.42
	15	0.7	0.4	0.3	492	0.26, 0.40
	20	0.9	0.6	0.4	500	0.28, 0.43

[a] CIE coordinates are taken at a current density of 100 cd m^{-2}.

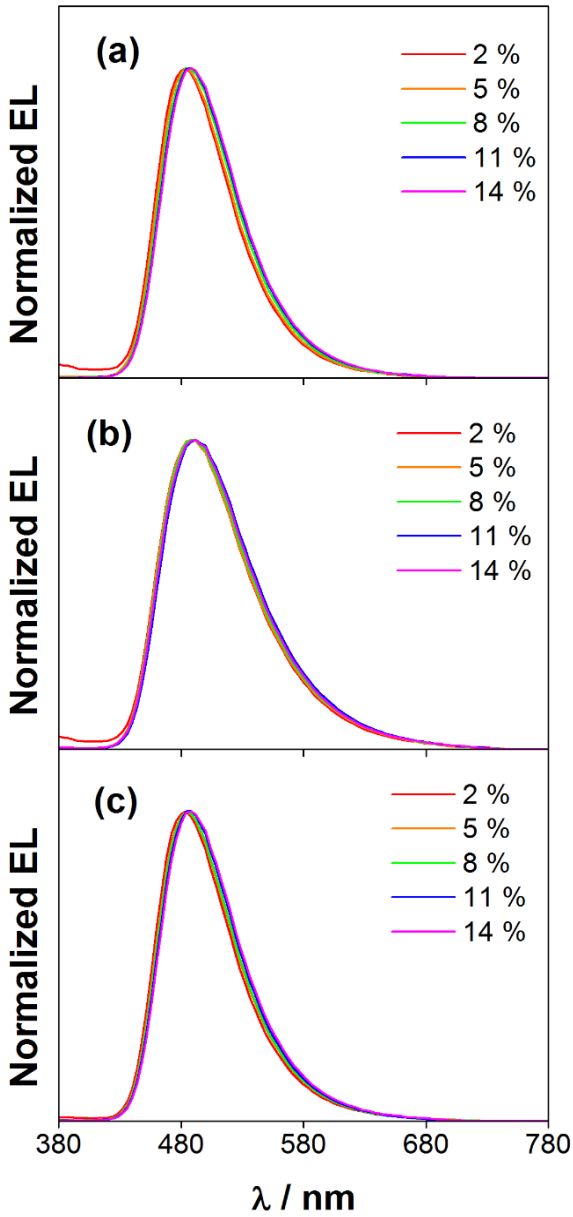

Figure S26. Normalized EL spectra of the vacuum-deposited OLEDs based on **1**–**3**.

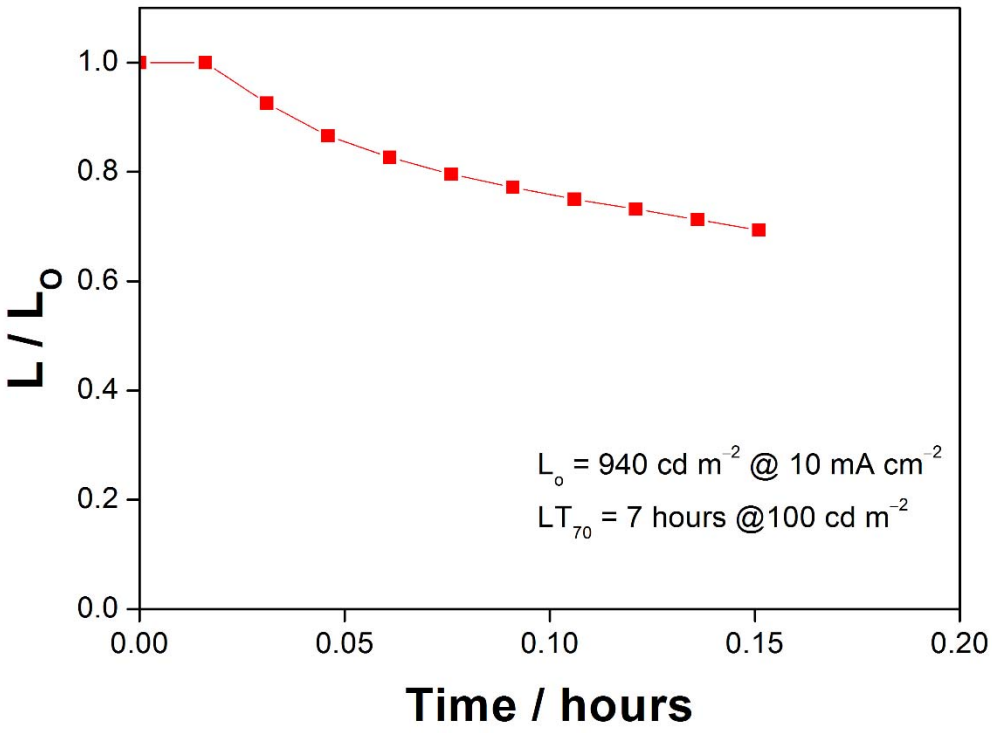

Figure S27. Operational lifetime of the vacuum-deposited device based on **1** at a constant driving current density of 10 mA cm^{-2}.

Supplementary references

1. Crosby, G. A.; Demas, J. N. Measurement of Photoluminescence Quantum Yields. Review. *J. Phys. Chem.* **1971**, *75*, 991–1024.
2. Sheldrick, G. M. *SHELXT* – Integrated Space-Group and Crystal-Structure Determination. *Acta Crystallogr A Found Adv* **2015**, *71*, 3–8.
3. Frisch, M. J. T., G. W.; Schlegel, H. B.; Scuseria, G. E.; Robb, M. A.; Cheeseman, J. R.; Scalmani, G.; Barone, V.; Mennucci, B.; Petersson, G. A.; Nakatsuji, H.; Caricato, M.; Li, X.; Hratchian, H. P.; Izmaylov, A. F.; Bloino, J.; Zheng, G.; Sonnenberg, J. L.; Hada, M.; Ehara, M.; Toyota, K.; Fukuda, R.; Hasegawa, J.; Ishida, M.; Nakajima, T.; Honda, Y.; Kitao, O.; Nakai, H.; Vreven, T.; Montgomery, J. A., Jr.; Peralta, J. E.; Ogliaro, F.; Bearpark, M.; Heyd, J. J.; Brothers, E.; Kudin, K. N.; Staroverov, V. N.; Keith, T.; Kobayashi, R.; Normand, J.; Raghavachari, K.; Rendell, A.; Burant, J. C.; Iyengar, S. S.; Tomasi, J.; Cossi, M.; Rega, N.; Millam, J. M.; Klene, M.; Knox, J. E.; Cross, J. B.; Bakken, V.; Adamo, C.; Jaramillo, J.; Gomperts, R.; Stratmann, R. E.; Yazyev, O.; Austin, A. J.; Cammi, R.; Pomelli, C.; Ochterski, J. W.; Martin, R. L.; Morokuma, K.; Zakrzewski, V. G.; Voth, G. A.; Salvador, P.; Dannenberg, J. J.; Dapprich, S.; Daniels, A. D.; Farkas, O.; Foresman, J. B.; Ortiz, J. V.; Cioslowski, J.; Fox, D. J. Gaussian 09, Revision D.01; Gaussian, Inc.: Wallingford, CT, 2013.
4. Perdew, J. P.; Burke, K.; Ernzerhof, M. Generalized Gradient Approximation Made Simple. *Phys. Rev. Lett.* **1996**, *77*, 3865–3868.
5. Perdew, J. P.; Burke, K.; Ernzerhof, M. Generalized Gradient Approximation Made Simple [Phys. Rev. Lett. 77, 3865 (1996)]. *Phys. Rev. Lett.* **1997**, *78*, 1396.
6. Adamo, C.; Barone, V. Toward Reliable Density Functional Methods Without Adjustable Parameters: The PBE0 Model. *J. Chem. Phys.* **1999**, *110*, 6158–6170.
7. Cossi, M.; Rega, N.; Scalmani, G.; Barone, V. Energies, Structures, and Electronic Properties of Molecules in Solution with the C-PCM Solvation Model. *J. Comput. Chem.* **2003**, *24*, 669–681.
8. Bauernschmitt, R.; Ahlrichs, R. Treatment of Electronic Excitations Within the Adiabatic Approximation of Time Dependent Density Functional Theory. *Chem. Phys. Lett.* **1996**, *256*, 454–464.
9. Casida, M. E.; Jamorski, C.; Casida, K. C.; Salahub, D. R. Molecular Excitation Energies to High-Lying Bound States from Time-Dependent Density-Functional

Response Theory: Characterization and Correction of the Time-Dependent Local Density Approximation Ionization Threshold. *J. Chem. Phys.* **1998**, *108*, 4439–4449.

10. Stratmann, R. E.; Scuseria, G. E.; Frisch, M. J. An Efficient Implementation of Time-Dependent Density-Functional Theory for the Calculation of Excitation Energies of Large Molecules. *J. Chem. Phys.* **1998**, *109*, 8218–8224.
11. Andrae, D.; Häußermann, U.; Dolg, M.; Stoll, H.; Preuß, H. Energy-Adjusted ab initio Pseudopotentials for the Second and Third Row Transition Elements. *Theor. Chim. Acta* **1990**, *77*, 123–141.
12. Ehlers, A. W.; Böhme, M.; Dapprich, S.; Gobbi, A.; Höllwarth, A.; Jonas, V.; Köhler, K. F.; Stegmann, R.; Veldkamp, A.; Frenking, G. A Set of F-Polarization Functions for Pseudo-Potential Basis Sets of the Transition Metals Sc–Cu, Y–Ag and La–Au. *Chem. Phys. Lett.* **1993**, *208*, 111–114.
13. Hehre, W. J.; Ditchfield, R.; Pople, J. A. Self-Consistent Molecular Orbital Methods. XII. Further Extensions of Gaussian-Type Basis Sets for Use in Molecular Orbital Studies of Organic Molecules. *J. Chem. Phys.* **1972**, *56*, 2257–2261.
14. Hariharan, P. C.; Pople, J. A. The Influence of Polarization Functions on Molecular Orbital Hydrogenation Energies. *Theor. Chim. Acta* **1973**, *28*, 213–222.
15. Francl, M. M.; Pietro, W. J.; Hehre, W. J.; Binkley, J. S.; Gordon, M. S.; DeFrees, D. J.; Pople, J. A. Self-Consistent Molecular Orbital Methods. XXIII. A Polarization-Type Basis Set for Second-Row Elements. *J. Chem. Phys.* **1982**, *77*, 3654–3665.
16. Tang, M.-C.; Lee, C.-H.; Lai, S.-L.; Ng, M.; Chan, M.-Y.; Yam, V. W.-W. Versatile Design Strategy for Highly Luminescent Vacuum-Evaporable and Solution-Processable Tridentate Gold(III) Complexes with Monoaryl Auxiliary Ligands and Their Applications for Phosphorescent Organic Light Emitting Devices. *J. Am. Chem. Soc.* **2017**, *139*, 9341–9349.
17. Wong, K. M.-C.; Hung, L.-L.; Lam, W. H.; Zhu, N.; Yam, V. W.-W. A Class of Luminescent Cyclometalated Alkynylgold(III) Complexes: Synthesis, Characterization, and Electrochemical, Photophysical, and Computational Studies of [Au(C^N^C)(C≡C–R)] (C^N^C = κ^3C,N,C Bis-cyclometalated 2,6-Diphenylpyridyl). *J. Am. Chem. Soc.* **2007**, *129*, 4350–4365.
18. Au, V. K.-M.; Tsang, D. P.-K.; Wong, K. M.-C.; Chan, M.-Y.; Zhu, N.; Yam, V. W.-W. Functionalized Bis-cyclometalated Alkynylgold(III) Complexes: Synthesis,

Characterization, Electrochemistry, Photophysics, Photochemistry, and Electroluminescence Studies. *Inorg. Chem.* **2013**, *52*, 12713–12725.